INTEGRAL TRANSFORMS SOLUTION FOR FLOW DEVELOPMENT IN WAVY WALL DUCTS

Roseane L. Silva
Mining Engineering Department, CSSPA
Universidade Federal do Pará, UFPA
Campus II, Folha 17, Quadra 04, Lote Especial, 68505–080, Marabá, PA, Brazil
roselima@ufpa.br

João N. N. Quaresma
School of Chemical Engineering
Universidade Federal do Pará, UFPA
Campus Universitário do Guamá, Rua Augusto Corrêa, 01, 66075–110, Belém, PA, Brazil
quaresma@ufpa.br

Carlos A. C. Santos
Solar Energy Laboratory, LES, Mechanical Engineering Department, DTM
Universidade Federal da Paraíba, UFPB
Cidade Universitária, 58059–900, João Pessoa, PB, Brazil
cabral@les.ufpb.br

Renato M. Cotta
Laboratory of Transmission and Technology of Heat–LTTC
Mechanical Engineering Department – POLI&COPPE/UFRJ
Universidade Federal do Rio de Janeiro, UFRJ
Cx. Postal 68503 – Cidade Universitária, 21945–970, Rio de Janeiro, RJ, Brazil
cotta@mecanica.coppe.ufrj.br

INTEGRAL TRANSFORMS SOLUTION FOR FLOW DEVELOPMENT IN WAVY WALL DUCTS

Abstract

Purpose - The present paper provides an analysis of two–dimensional laminar flow in the entrance region of wavy–wall ducts as obtained from the solution of the steady Navier–Stokes equations for incompressible flow.
Design/methodology/approach - The study is undertaken by application of the Generalized Integral Transform Technique (GITT) in the solution of the steady Navier–Stokes equations for incompressible flow. The streamfunction–only formulation is adopted, and a general filtering solution that adapts to the irregular contour is proposed to enhance the convergence behavior of the eigenfunction expansion.
Findings - A few representative cases are considered more closely in order to report some numerical results illustrating the eigenfunction expansions convergence behavior. The product friction factor–Reynolds number is also computed and compared against results from discrete methods available in the literature for different Reynolds numbers and amplitudes of the wavy channel.
Research limitations/applications - The proposed methodology is fairly general in the analysis of different channel profiles, though the reported results are limited to the wavy channel configuration. Future work should also extend the analysis to geometries represented in the cylindrical coordinates with longitudinally variable radius.
Practical implications - The error controlled converged results provide reliable benchmark results for the validation of numerical results from computational codes that address the solution of the Navier-Stokes equations in irregular geometries.
Originality/value - Although the hybrid methodology is already known in the literature, the results here presented are original and further challenges application of the integral transform method in the solution of the Navier-Stokes equations.

Keywords: Navier–Stokes equations, wavy–wall channels, integral transforms, friction factor, hybrid methods.

Nomenclature

a^*	amplitude of the wavy boundary
b	half the distance between the walls at the duct inlet
c	parameter of scale compression
F(x,y)	filtering function
k_1, k_2	streamfunction values at the duct walls
n	unit normal vector
N_i	norm
NTV	expansion truncation order
p	dimensionless pressure field
Q	dimensionless mass flux
Re	Reynolds number
u	dimensionless longitudinal velocity component
v	dimensionless transversal velocity component
x	dimensionless longitudinal coordinate
x_{out}	value of the longitudinal coordinate at the duct outlet
y	dimensionless transversal coordinate
y_1, y_2	boundaries geometric profiles
Y_i	eigenfunctions

Greek letters

α	dimensionless duct amplitude
β_i	x–independent eigenvalues
η	transformed longitudinal coordinate
ξ	transformed transversal coordinate
τ	compressed longitudinal coordinate
ϕ	filtered potential
$\bar{\phi}_i$	transformed potentials
ψ	streamfunction
ω	vorticity

Subscripts and superscripts

_	integral transformed quantities
i, j, k	expansions indices

1. Introduction

Fluid flow within irregularly shaped ducts is found in several industrial applications related, for instance, to the flow of liquids in chemical processing plants, air flow in cooling, heating and ventilation units, and cooling of electronic equipment. In these applications there is the need of evaluating certain physical parameters for proper thermal–hydraulic design, such as friction factors and heat transfer coefficients. Channels with corrugated surfaces are, for example, employed in compact heat exchangers [1] for heat transfer enhancement. Most theoretical studies performed on the fluid dynamics and thermal phenomena occurring in corrugated wall ducts consider corrugations having a periodical pattern which are described by simple functions such as rectangular, triangular or sinusoidal relations. A few experimental and theoretical studies are available in the literature on the thermohydraulics of such wavy wall ducts [2–6]. Wall corrugation may also be employed aimed at promoting early transition of laminar to turbulent flows, sometimes responsible for the enhancement of heat transfer in practical applications [7-10]. More recently, a few works have addressed the interest in investigating channel corrugations at the micro-scale, either for liquid or gaseous flows [11-13].

The numerical simulation of flows in irregularly shaped channels by the conventional discrete approaches requires sufficiently fine meshes and considerable computational effort so as to capture the detailed aspects of the fluid flow that influence the wall friction. On the other hand, a number of hybrid numerical–analytical approaches were progressively developed and presented in the open literature, advocated as less expensive and at least as companion tools for the more popular and, in general, more straightforward discrete numerical methods. Eigenfunction expansion–type approaches were among such extended analytical tools that to a considerable extent were also able to profit from the concurrent development of symbolic computation platforms [14]. Within this class of approaches, the Integral Transform Method was gradually expanded in its applicability, under the label of the Generalized Integral Transform Technique (GITT) [15–21], and extensively employed in heat/mass transfer and fluid flow problems. For instance, under either the boundary layer or full Navier–Stokes formulations, a number of contributions have advanced this method towards the error controlled solution of internal flow and convective heat transfer problems [22–37]. Both the primitive variables and streamfunction (or vector–scalar potentials for three–dimensional flows) formulations were adopted in such developments, with some preference to the streamfunction form, due to the elimination of the pressure field and automatic satisfaction of the continuity equation. In the case of the streamfunction–only formulation, the appropriate eigenfunction expansion for the velocity problem is in general proposed based on a fourth order eigenvalue problem related to the analytical solution of the linear biharmonic equation for vanishing Reynolds number. In the context of computational solutions with automatically controlled accuracy, the Generalized Integral Transform Technique (GITT) [14–21], with its automatic global error control capability, appears as a reliable path for obtaining benchmark results, allowing for a more definitive critical evaluation of previously published numerical results of classical test problems. The GITT has already been utilized to find hybrid analytical–numerical solutions for laminar flow development inside parallel–plates channels [23–26, 35], by using both the primitive variables and streamfunction–only formulations, in either the Navier–Stokes or boundary layer formulations. Extending such efforts, the present work is motivated by the application of the GITT in the solution of hydrodynamic developing flow in a wavy wall duct. Thus, a Navier–Stokes–based formulation for two–dimensional laminar incompressible flow in irregularly shaped channels is adopted, in terms of the streamfunction only such as that one originally proposed and solved by integral transforms in [34]. Here, the streamfunction is split up in two parts, where one of them represents a generic

filtering solution, which adapts to the irregular boundary of the duct. The aim of the filtering solution is to offer a convergence enhancement effect on the eigenfunction expansion for the streamfunction, by utilizing an analytical filter that changes along the flow development. A wavy wall duct is then more closely studied and computations for the streamfunction, vorticity and velocity fields are performed, as well as for the product of the friction factor–Reynolds number, for different values of the governing parameters of the flow, such as the Reynolds number and the amplitude of the wavy surface, extending the scope and preliminary assessment of this problem as first presented in [38]. Finally, a set of reference results are systematically presented and employed to covalidate previously reported results [6] obtained by discrete numerical methods.

2. Problem formulation and solution methodology

We consider two–dimensional steady laminar flow of an incompressible Newtonian fluid in the inlet region of a duct of irregular geometry. Figure 1 shows the schematic representation of the considered internal flow problem, which is not required to be symmetrical with respect to the longitudinal axis in the proposed approach and associated algorithm. The flow is governed by the continuity and Navier–Stokes equations, and the following dimensionless variables are here employed:

$$\begin{aligned} &x = x^* / b;\ y = y^* / b;\ y_1(x) = y_1^*(x^*) / b;\ y_2(x) = y_2^*(x^*) / b; \\ &u = u^* / u_0;\ v = v^* / u_0;\ p = p^* / \rho u_0^2;\ Re = b u_0 / \nu \end{aligned} \tag{1a–h}$$

where b represents half the distance between the walls at the duct inlet.

Adopting the streamfunction–only formulation [34], the problem is then written in dimensionless form as:

$$L_1[\psi, \psi] = L_2[\psi] \tag{2a}$$

the operators $L_1[f, g]$ and $L_2[f]$ are defined as

$$L_1[f,g] = \frac{\partial f}{\partial y}\left(\frac{\partial^3 g}{\partial x^3} + \frac{\partial^3 g}{\partial x \partial y^2}\right) - \frac{\partial f}{\partial x}\left(\frac{\partial^3 g}{\partial x^2 \partial y} + \frac{\partial^3 g}{\partial y^3}\right) \tag{2b}$$

$$L_2[f] = \frac{1}{Re}\left(\frac{\partial^4 f}{\partial x^4} + 2\frac{\partial^4 f}{\partial x^2 \partial y^2} + \frac{\partial^4 f}{\partial y^4}\right) \tag{2c}$$

and the boundary conditions are associated with no–slip and impermeability at the duct walls.

$$\psi(x, -y_1(x)) = k_1; \quad \frac{\partial \psi(x, -y_1(x))}{\partial \mathbf{n}} = 0 \tag{3a,b}$$

$$\psi(x, y_2(x)) = k_2; \quad \frac{\partial \psi(x, y_2(x))}{\partial \mathbf{n}} = 0 \tag{4a,b}$$

where **n**, k_1 and k_2 represent, respectively, the unit normal vector in the outward direction of the duct wall and the streamfunction values at the walls. The constant Q represents the volumetric flow rate per unit of length and is determined as [34]:

$$\psi(0, y_2) = k_2 = Q + k_1 \tag{5}$$

In the above equations the definition of streamfunction was employed according to:

$$u(x,y) = \frac{\partial \psi(x,y)}{\partial y}, \quad v(x,y) = -\frac{\partial \psi(x,y)}{\partial x} \tag{6a,b}$$

These definitions allow automatic satisfaction of the continuity equation and eliminate the pressure field from the problem formulation, Eq. (2a).

In the solution of Eq. (2a) by using the GITT approach, it is convenient to define a filter in order to homogenize the boundary conditions in the y direction, which later will be the coordinate chosen for construction of the eigenvalue problem. Therefore, the general filtering function is defined from:

$$\psi(x,y) = \phi(x,y) + F(x,y) \tag{7}$$

where $\phi(x,y)$ represents the unknown potential to be determined, and $F(x,y)$ is the filter, which at this point is only required to have the same values of $\psi(x,y)$ at the duct walls. The function $F(x,y)$ is thus not necessarily a particular solution of $\psi(x,y)$. Therefore, introducing Eq. (7) into Eq. (2a), results

$$L_1[\phi,\phi] + L_1[\phi,F] + L_1[F,\phi] + L_1[F,F] = L_2[\phi] + L_2[F] \tag{8}$$

with the filtered boundary conditions

$$\phi(x,-y_1) = k_1 - F(x,-y_1); \quad \frac{\partial \phi(x,-y_1)}{\partial \mathbf{n}} = 0 \tag{9a,b}$$

$$\phi(x,y_2) = k_2 - F(x,y_2); \quad \frac{\partial \phi(x,y_2)}{\partial \mathbf{n}} = 0 \tag{10a,b}$$

The filtering function can be built, for instance, by constructing at any cross–section along the duct a fully developed velocity profile, which follows the irregularity of the duct. In order to more easily obtain this filter, a relationship between the original coordinates system (y,x) and a new transformed system (η,x) is given as:

$$\eta = y - y_3(x); \quad y_0(x) = \frac{1}{2}\left[y_1(x) + y_2(x)\right]; \quad y_3(x) = \frac{1}{2}\left[y_2(x) - y_1(x)\right] \tag{11a–c}$$

or in terms of the original coordinates

$$F(x,y) = \frac{3}{4} Q \left[\left(\frac{y - y_3}{y_0} \right) - \frac{1}{3} \left(\frac{y - y_3}{y_0} \right)^3 \right] + \frac{Q}{2} + k_1 \tag{12}$$

where y_3 represents the distance between the axes y and η, while y belongs to the interval $[-y_1(x), y_2(x)]$ and $\eta \in [-y_0(x), y_0(x)]$. On the other hand, a fixed domain permits a more straightforward visualization of both this filtering solution and the eigenvalue problem to be proposed, in terms of a new transversal coordinate, ξ. Therefore the domain $\xi \in [-1,1]$ is defined from:

$$\xi = \frac{\eta}{y_0} = \frac{y - y_3}{y_0} \tag{13}$$

Thus, the filter can be rewritten in the form

$$F(\xi) = \frac{3}{4} \left[\xi - \frac{\xi^3}{3} \right] + \frac{Q}{2} + k_1 \tag{14}$$

Now, in light of the homogeneous characteristics of the boundary conditions in the transversal direction, it is more appropriate to choose this coordinate for proposing the eigenfunction expansion, to be employed in the process of integral transformation. By considering the relation given by Eq. (13), the auxiliary fourth order eigenvalue problem is taken as:

$$\frac{d^4Y_i(\xi)}{d\xi^4}=(\mu_i y_0)^4 Y_i(\xi)\equiv\beta_i^4 Y_i(\xi) \tag{15a}$$

$$Y_i(-1)=0;\quad \frac{dY_i(-1)}{d\xi}=0;\quad Y_i(1)=0;\quad \frac{dY_i(1)}{d\xi}=0 \tag{15b–e}$$

Problem (15) is analytically solved, to furnish

$$Y_i(\xi)=\begin{cases}\dfrac{\cos(\beta_i\xi)}{\cos(\beta_i)}-\dfrac{\cosh(\beta_i\xi)}{\cosh(\beta_i)}, & i=1,3,5,...\\ \dfrac{\sin(\beta_i\xi)}{\sin(\beta_i)}-\dfrac{\sinh(\beta_i\xi)}{\sinh(\beta_i)}, & i=2,4,6,...\end{cases} \tag{16}$$

where the x–independent eigenvalue β_i is defined as, $\beta_i=\mu_i(x)y_0(x)$, and computed from the transcendental equations below

$$\tanh(\beta_i)=\begin{cases}-\tan(\beta_i), & i=1,3,5,...\\ \tan(\beta_i), & i=2,4,6,...\end{cases} \tag{17}$$

Also, the eigenfunctions satisfy the following orthogonality property:

$$\int_{-y_1}^{y_2} Y_i Y_j dy=\begin{cases}0, & \text{for}\quad i\neq j\\ N_i(x)=2y_0(x), & \text{for}\quad i=j\end{cases} \tag{18a,b}$$

where $N_i(x)$ is the normalization integral and the index i in Eq.(18.b) can thus be dropped.

The eigenvalue problem defined by Eqs.(15) allows for the definition of the following integral transform pair:

$$\bar{\phi}_i(x)=\frac{1}{N(x)}\int_{-y_1}^{y_2} Y_i(x,y)\phi(x,y)dy,\quad \text{transform} \tag{19}$$

$$\phi(x,y)=\sum_{i=1}^{\infty} Y_i(x,y)\bar{\phi}_i(x),\quad \text{inverse} \tag{20}$$

We can now accomplish the integral transformation of the original partial differential system given by Eqs. (8)–(10). For this purpose, Eq. (8) is multiplied by Y_i and is then integrated over the domain $[-y_1(x),y_2(x)]$ in y. After that, the inverse formula given by Eq. (20) is employed, resulting after some manipulations in the following coupled ordinary differential system for the calculation of the transformed potentials $\bar{\phi}_i$:

$$\overline{\phi}_i^{(iv)} = -\mu_i^4\overline{\phi}_i + \frac{L_i}{N} + \frac{Re}{N}\sum_{j=1}^{\infty}\sum_{k=1}^{\infty}\Big\{ A_{ijk}\overline{\phi}_j\overline{\phi}_k + B_{ijk}\overline{\phi}_j\overline{\phi}_k' + C_{ijk}\overline{\phi}_j\overline{\phi}_k'' + D_{ijk}\overline{\phi}_j\overline{\phi}_k'''$$

$$+E_{ijk}\overline{\phi}_j'\overline{\phi}_k + F_{ijk}\overline{\phi}_j'\overline{\phi}_k' + G_{ijk}\overline{\phi}_j'\overline{\phi}_k'' \Big\} + \frac{1}{N}\sum_{j=1}^{\infty}\Big\{ H_{ij}\overline{\phi}_j + I_{ij}\overline{\phi}_j' + J_{ij}\overline{\phi}_j'' + K_{ij}\overline{\phi}_j''' \Big\} \qquad (21)$$

The outflow boundary conditions are here chosen from two possibilities. In the first one, the duct is considered to be finite (truncated duct), and the following boundary conditions are employed:

$$v(x_{out}, y) = 0; \quad \frac{\partial\omega(x_{out}, y)}{\partial x} = 0 \qquad (22a,b)$$

where ω is the vorticity.

The second possibility considers that the duct is infinite. Therefore, when $x\to\infty$, the outflow boundary conditions are those of a fully developed flow in a parallel-plates channel, which are given by:

$$u(\infty, y) = \frac{3}{2}(1-y^2); \quad v(\infty, y) = 0 \qquad (23a,b)$$

The boundary conditions given by Eqs. (22) and (23), after introducing the definition of the streamfunction, Eqs. (6), and the general filtering function given by Eq. (7), are rewritten as:

– For a truncated duct

$$\frac{\partial\phi(x_{out}, y)}{\partial x} + \frac{\partial F(x_{out}, y)}{\partial x} = 0 \qquad (24a)$$

$$\frac{\partial^3\phi(x_{out}, y)}{\partial x^3} + \frac{\partial^3\phi(x_{out}, y)}{\partial x\partial y^2} + \frac{\partial^3 F(x_{out}, y)}{\partial x^3} + \frac{\partial^3 F(x_{out}, y)}{\partial x\partial y^2} = 0 \qquad (24b)$$

– For an infinite duct

$$\phi(\infty, y) = 0 \qquad (25a)$$

$$\frac{\partial\phi(\infty, y)}{\partial x} = 0 \qquad (25b)$$

Now, the integral transformation process of Eqs. (24) and (25) is similar to that of obtaining Eq. (21), i.e., the equations are multiplied by Y_i and then integrated over the domain $[-y_1(x), y_2(x)]$ in y. After that, the inverse formula given by Eq. (20) is employed, yielding:

– For a truncated duct

$$\overline{\phi}_i(0) = 0; \quad \frac{d\overline{\phi}_i(0)}{dx} = 0 \qquad (26a,b)$$

$$\frac{d\bar{\phi}_i(x_{out})}{dx} = -\frac{1}{N(x_{out})}\left[M_i + \sum_{j=1}^{\infty} N_{ij}\bar{\phi}_j(x_{out})\right] \tag{26c}$$

$$\frac{d^3\bar{\phi}_i(x_{out})}{dx^3} = -\frac{1}{N(x_{out})}\left\{O_i + \sum_{j=1}^{\infty}\left[P_{ij}\bar{\phi}_j(x_{out}) + Q_{ij}\frac{d\bar{\phi}_j(x_{out})}{dx} + R_{ij}\frac{d^2\bar{\phi}_j(x_{out})}{dx^2}\right]\right\} \tag{26d}$$

– For an infinite duct

$$\bar{\phi}_i(0) = 0; \quad \frac{d\bar{\phi}_i(0)}{dx} = 0; \quad \bar{\phi}_i(\infty) = 0; \quad \frac{d\bar{\phi}_i(\infty)}{dx} = 0 \tag{27a–d}$$

The coefficients that depend on x are calculated from:

$$A_{ijk} = \int_{-y_1}^{y_2} Y_i\left[\frac{\partial Y_j}{\partial y}\left(\frac{\partial^3 Y_k}{\partial x^3} + \frac{\partial^3 Y_k}{\partial x \partial y^2}\right) - \frac{\partial Y_j}{\partial x}\left(\frac{\partial^3 Y_k}{\partial x^2 \partial y} + \frac{\partial^3 Y_k}{\partial y^3}\right)\right]dy \tag{28a}$$

$$B_{ijk} = \int_{-y_1}^{y_2} Y_i\left[\frac{\partial Y_j}{\partial y}\left(3\frac{\partial^2 Y_k}{\partial x^2} + \frac{\partial^2 Y_k}{\partial y^2}\right) - 2\frac{\partial Y_j}{\partial x}\frac{\partial^2 Y_k}{\partial x \partial y}\right]dy \tag{28b}$$

$$C_{ijk} = \int_{-y_1}^{y_2} Y_i\left[3\frac{\partial Y_j}{\partial y}\frac{\partial Y_k}{\partial x} - \frac{\partial Y_j}{\partial x}\frac{\partial Y_k}{\partial y}\right]dy \tag{28c}$$

$$D_{ijk} = \int_{-y_1}^{y_2} Y_i\frac{\partial Y_j}{\partial y}Y_k dy; \quad E_{ijk} = -\int_{-y_1}^{y_2} Y_i Y_j\left[\frac{\partial^3 Y_k}{\partial x^2 \partial y} + \frac{\partial^3 Y_k}{\partial y^3}\right]dy \tag{28d,e}$$

$$F_{ijk} = -2\int_{-y_1}^{y_2} Y_i Y_j\frac{\partial^2 Y_k}{\partial x \partial y}dy; \quad G_{ijk} = -\int_{-y_1}^{y_2} Y_i Y_j\frac{\partial Y_k}{\partial y}dy \tag{28f,g}$$

$$H_{ij} = a_{ij}Re - b_{ij}; \quad I_{ij} = c_{ij}Re - d_{ij}; \quad J_{ij} = e_{ij}Re - f_{ij}; \quad K_{ij} = g_{ij}Re - h_{ij}; \quad L_i = i_i Re - j_i \tag{28h–l}$$

$$M_i = \int_{-y_1}^{y_2} Y_i\frac{\partial F}{\partial x}dy; \quad N_{ij} = \int_{-y_1}^{y_2} Y_i\frac{\partial Y_j}{\partial x}dy \tag{28m,n}$$

$$O_i = \int_{-y_1}^{y_2} Y_i\left[\frac{\partial^3 F}{\partial x^3} + \frac{\partial^3 F}{\partial x \partial y^2}\right]dy; \quad P_{ij} = \int_{-y_1}^{y_2} Y_i\left[\frac{\partial^3 Y_j}{\partial x^3} + \frac{\partial^3 Y_j}{\partial x \partial y^2}\right]dy \tag{24o,p}$$

$$Q_{ij} = \int_{-y_1}^{y_2} Y_i\left[3\frac{\partial^2 Y_j}{\partial x^2} + \frac{\partial^2 Y_j}{\partial y^2}\right]dy; \quad R_{ij} = 3\int_{-y_1}^{y_2} Y_i\frac{\partial Y_j}{\partial x}dy \tag{28q,r}$$

$$a_{ij} = \int_{-y_1}^{y_2} Y_i\left[\frac{\partial Y_j}{\partial y}\left(\frac{\partial^3 F}{\partial x^3} + \frac{\partial^3 F}{\partial x \partial y^2}\right) - \frac{\partial Y_j}{\partial x}\left(\frac{\partial^3 F}{\partial x^2 \partial y} + \frac{\partial^3 F}{\partial y^3}\right) + \left(\frac{\partial^3 Y_j}{\partial x^3} + \frac{\partial^3 Y_j}{\partial x \partial y^2}\right)\frac{\partial F}{\partial y} - \left(\frac{\partial^3 Y_j}{\partial x^2 \partial y} + \frac{\partial^3 Y_j}{\partial y^3}\right)\frac{\partial F}{\partial x}\right]dy; \tag{29a}$$

$$b_{ij} = \int_{-y_1}^{y_2} Y_i\left[\frac{\partial^4 Y_j}{\partial x^4} + 2\frac{\partial^4 Y_j}{\partial x^2 \partial y^2}\right]dy \tag{29b}$$

$$c_{ij} = \int_{-y_1}^{y_2} Y_i\left[Y_j\left(-\frac{\partial^3 F}{\partial x^2 \partial y} - \frac{\partial^3 F}{\partial y^3}\right) + \left(3\frac{\partial^2 Y_j}{\partial x^2} + \frac{\partial^2 Y_j}{\partial y^2}\right)\frac{\partial F}{\partial y} - 2\frac{\partial^2 Y_j}{\partial x \partial y}\frac{\partial F}{\partial x}\right]dy \tag{29c}$$

$$d_{ij} = 4\int_{-y_1}^{y_2} Y_i \left[\frac{\partial^3 Y_j}{\partial x^3} + \frac{\partial^3 Y_j}{\partial x \partial y^2} \right] dy \; ; \quad e_{ij} = \int_{-y_1}^{y_2} Y_i \left[3\frac{\partial Y_j}{\partial x}\frac{\partial F}{\partial y} - \frac{\partial Y_j}{\partial y}\frac{\partial F}{\partial x} \right] dy \qquad (29d,e)$$

$$f_{ij} = 2\int_{-y_1}^{y_2} Y_i \left[3\frac{\partial^2 Y_j}{\partial x^2} + \frac{\partial^2 Y_j}{\partial y^2} \right] dy \; ; \quad g_{ij} = \int_{-y_1}^{y_2} Y_i Y_j \frac{\partial F}{\partial y} dy \; ; \quad h_{ij} = 4\int_{-y_1}^{y_2} Y_i \frac{\partial Y_j}{\partial x} dy \qquad (29f\text{-}h)$$

$$i_i = \int_{-y_1}^{y_2} Y_i \left(\frac{\partial F}{\partial y}\frac{\partial^3 F}{\partial x^3} + \frac{\partial F}{\partial y}\frac{\partial^3 F}{\partial x \partial y^2} - \frac{\partial F}{\partial x}\frac{\partial^3 F}{\partial x^2 \partial y} - \frac{\partial F}{\partial x}\frac{\partial^3 F}{\partial y^3} \right) dy \; ; \; j_i = \int_{-y_1}^{y_2} Y_i \left(\frac{\partial^4 F}{\partial x^4} + 2\frac{\partial^4 F}{\partial x^2 \partial y^2} \right) dy \qquad (29i,j)$$

For computational purposes, it is necessary to truncate the infinite expansions in a sufficiently large number of terms so as to achieve the user prescribed relative error target for obtaining the original potentials, in this case the streamfunction values, where NTV is here the order of truncation of the infinite series. Also, in order to solve the transformed ODE system, efficient numerical algorithms for boundary value problems are to be employed, such as the subroutine DBVPFD from the IMSL Library [39], which offers an automatic adaptive scheme for local error control of the numerical results for the transformed potentials. It is then necessary to rewrite the transformed ODE system as a first order one, by introducing the following dependent variables:

$$\chi_i = \bar{\phi}_i \; ; \quad \frac{d\chi_i}{dx} = \chi_{NTV+i} = \frac{d\bar{\phi}_i}{dx} \; ; \quad \frac{d\chi_{NTV+i}}{dx} = \chi_{2NTV+i} = \frac{d^2\bar{\phi}_i}{dx^2} \; ;$$
$$\frac{d\chi_{2NTV+i}}{dx} = \chi_{3NTV+i} = \frac{d^3\bar{\phi}_i}{dx^3} \; ; \quad \frac{d\chi_{3NTV+i}}{dx} = \frac{d^4\bar{\phi}_i}{dx^4} \qquad (30a\text{–}e)$$

Therefore, by making use of Eqs. (30), the transformed system can be rewritten as:

$$\frac{d\chi_i}{d\tau} = \frac{\chi_{NTV+i}}{\left(\frac{d\tau}{dx}\right)} \; ; \quad \frac{d\chi_{NTV+i}}{d\tau} = \frac{\chi_{2NTV+i}}{\left(\frac{d\tau}{dx}\right)} \; ; \quad \frac{d\chi_{2NTV+i}}{d\tau} = \frac{\chi_{3NTV+i}}{\left(\frac{d\tau}{dx}\right)} \qquad (31a\text{–}c)$$

$$\frac{d\chi_{3NTV+i}}{d\tau} = \left\{ -\mu_i^4 \chi_i + \frac{L_i}{N} + \frac{Re}{N} \sum_{j=1}^{NTV} \sum_{k=1}^{NTV} \left[A_{ijk}\chi_j\chi_k + B_{ijk}\chi_j\chi_{NTV+k} \right.\right.$$
$$\left. + C_{ijk}\chi_j\chi_{2NTV+k} + D_{ijk}\chi_j\chi_{3NTV+k} + E_{ijk}\chi_{NTV+j}\chi_k + F_{ijk}\chi_{NTV+j}\chi_{NTV+k} + G_{ijk}\chi_{NTV+j}\chi_{2NTV+k} \right]$$
$$\left. + \frac{1}{N} \sum_{j=1}^{NTV} \left[H_{ij}\chi_j + I_{ij}\chi_{NTV+j} + J_{ij}\chi_{2NTV+j} + K_{ij}\chi_{3NTV+j} \right] \right\} \Big/ \left(\frac{d\tau}{dx}\right), \text{ for } i = 1,2,...,NTV \qquad (31d)$$

with $\tau = 1 - e^{-cx}$, $0 \le \tau \le 1$, and c being a parameter of scale compression for the case of an infinite duct.

Analyzing the ODE system given by Eqs. (31) we observe that the integral coefficients depend on the axial position x. This would imply in a high computational cost if the coefficients would require error controlled numerical integrations, once they need to be continuously reevaluated along the solution procedure for the ordinary differential equations system. However, all of them could be analytically determined through symbolic computation [14]. Also, the computational procedure is organized in such a way that the x–independent portions of each coefficient are calculated only once, before entering the boundary value problem solver, and stored. Along the ODE system integration, they are then recalled and

multiplied by the functions that take into account the dependence of the irregular domain as the differential system is being numerically solved.

3. Results and discussion

We analyze the wavy wall duct whose geometry was considered in ref. [6] and is shown schematically in Fig. 2 below. The functions that describe this symmetric geometry in dimensionless terms are given as

$$y_1(x) = 1 + f(x); \quad y_2(x) = 1 + f(x); \quad f(x) = \alpha \sin\left[\pi(x-3)\right] \qquad (32a–c)$$

where $\alpha = a^*/b$ is the dimensionless amplitude of the wavy surface, and the value of the axial coordinate at the duct outlet x_{out} was taken as $x_{out}=20$. In the present analysis, the interval used for the axial coordinate x was $3 \le x \le 15$, which corresponds to six complete sinusoidal waves.

Tables 1 to 3 show the convergence of the streamfunction values along the line y=0.5 for Re=100 and $\alpha=0.3$, Re=300 and $\alpha=0.2$, and Re=500 and $\alpha=0.1$, respectively, for the two cases of outflow boundary conditions (here named truncated duct and infinite duct, respectively). For the case of Re=100 and $\alpha=0.3$, it is observed that full convergence to four significant digits is achieved with NTV=18, while for the case Re=500 and $\alpha=0.1$, similar convergence is reached only with NTV=22. In Table 2, the results obtained with NTV=22 and 26 have remained unaffected, and the same happens in Table 3, though this is not evident from the previous column for NTV=18. The algorithm is organized so that numerical computation automatically ceases once the requested precision is achieved. In general, the results for the two cases of outflow boundary conditions analyzed are in perfect agreement, with a slight difference for axial positions near the duct outlet (x=20), which in terms of relative deviation is always below 0.5% for the fully converged results (NTV=22). This is justified by the fact that for the infinite duct, the fully developed region is not imposed and is reached at axial positions a little further away.

Figures 3(a)–(d) show a comparison of the present results for the product fRe with those numerically obtained by Wang and Chen [6] at different axial positions along the channel, for the cases Re=100 and $\alpha=0.2$, Re=300 and $\alpha=0.2$, Re=500 and $\alpha=0.1$ and Re=500 and $\alpha=0.2$, respectively. Wang and Chen [6] employed a coordinate transformation and the spline alternating–direction implicit method, an improved version of the cubic spline collocation method. One can see an excellent agreement among the four sets of results, obtained via two quite different solution methodologies, offering a fairly reliable covalidation report. Also, it can be verified how importantly the Reynolds number influences the product fRe, i.e., higher peaks are found for increasing Reynolds numbers and fixed duct geometry, indicating the evidently expected higher viscous effects in the flow. In both cases, the GITT results for the product fRe are already converged to the graph scale. In tabular form, a convergence rate of at least two significant digits for fRe is observed in most cases. The computation of the friction factor involves derivatives of the velocity field, which present a slower convergence behavior than the original expanded potentials. Also, one can notice negative values for the product fRe in some positions, which indicate the presence of recirculation zones. In addition, Fig. 4 shows the convergence behavior of the product fRe for the most severe case of Re=500 and $\alpha=0.3$, with different truncations orders NTV=13, 15, 17 and 19, in order to demonstrate the graphical convergence behavior of such results. This case brings a combination of the highest Reynolds number and duct amplitude considered in the present work; nevertheless, an excellent graphical convergence of fRe is also verified for this situation. Figures 5(a)–(c) show the product fRe for different values of the Reynolds number, respectively, Re=100, 300

and 500, and varying the dimensionless duct amplitude for each set of curves, so as to illustrate the effect of the duct geometry. Clearly, the fRe peaks are markedly affected by the increase in the amplitude of the sinusoidal oscillation on the boundary geometry, with the growing recirculation flow patterns, as will be more evident from the contour plots for the streamfunction in what follows.

As for the product fRe, Figure 6 shows the convergence behavior for the evolution of the axial component velocity at the duct centerline, u(x,0), for the more severe case of Re=500 and α=0.3, and again a reasonable graphical convergence rate is achieved for this parameter. Then, Figs. 7(a)–(c) illustrate the evolution of the axial component velocity at the duct centerline for different values of the dimensionless duct amplitude in each set of curves for Re=100, 300 and 500, respectively. As the Reynolds number and the duct amplitude increase, it is observed higher distortions in the longitudinal velocity component evolutions, demonstrating the increased perturbation on the core flow around the channel centerline. With the increase on the channel walls sinusoidal amplitude, the flow is noticeably accelerated in average terms along the centerline within this development region, as a direct result of the effective flow path periodic constriction.

Finally, Figures 8(a)–(c) to 10(a)–(c) show the isolines patterns of the streamfunction for all three values of Reynolds numbers and duct wall sinusoidal amplitudes here considered. The marked influence of the combined increase on Reynolds number and channel amplitude is clearly observable in the appearance of stronger recirculation zones internally to the "cavities" formed by the wavy walls. Specifically, the case of Re=500 and α=0.3 shows the strongest recirculation zone, even at the duct outlet, demonstrating the influence pointed out above.

4. Conclusions

The Generalized Integral Transform Technique (GITT) has been demonstrated in the hybrid numerical–analytical solution of laminar flow problems within channels with wavy walls. The case of a wavy–walls duct has been more closely considered in light of its importance in heat transfer enhancement applications. A steady two–dimensional formulation based on the Navier–Stokes equations and on the streamfunction definition is adopted. Employing a simple coordinate transformation, a straightforward filtering solution is then obtained, offering a relevant convergence enhancement effect in the eigenfunction expansion for the streamfuntion.

The convergence behavior of the proposed eigenfunction expansion is illustrated, and numerical results for the friction factor are critically compared with previously obtained numerical results from discrete approaches, with good agreement. A few additional results are also presented and employed in the interpretation of some physical aspects in this flow problem.

The proposed hybrid approach is fairly general and opens up several possibilities of analysis, including the search of optimized heat transfer surfaces forms under prescribed pressure drop requirements. Since the hybrid solution is fully analytical in the transversal direction, integrals and derivatives at any cross–section can be readily derived without further numerical involvement. The approach can also be quite interesting in the analysis of periodic fully developed situations.

Acknowledgments

The authors would like to acknowledge the partial financial support provided by the Brazilian agencies and programs, FADESP and CNPq. One of the authors (R.M.C.) is also grateful for the kind hospitality of the School of Chemical Engineering and Laboratory of Solar Energy, during his technical visits to, respectively, the Universidade Federal do Pará and Universidade Federal da Paraíba, in 2007 and 2008.

References

[1] Kays WM, London AL. Compact heat exchangers. New York: McGraw–Hill; 1984.
[2] Goldstein L, Sparrow EM. Heat/mass characteristics for flow in a corrugated wall channel. Journal of Heat Transfer 1977; **99**: 187–195.
[3] Asako Y, Nakamura H, Faghri M. Heat transfer and pressure drop characteristics in a corrugated duct with rounded corners. International Journal of Heat and Mass Transfer 1988; **31**: 1237–1245.
[4] Sunden B, Trollheden S. Periodic laminar flow and heat transfer in a corrugated two–dimensional channel. International Communications in Heat and Mass Transfer 1989; **16**: 215–225.
[5] Xiao Q, Xin RC, Tao WQ. Analysis of fully developed laminar flow and heat transfer in asymmetric wavy channels. International Communications in Heat and Mass Transfer 1989; **16**: 227–236.
[6] Wang CC, Chen CK. Forced convection in a wavy–wall channel. International Journal of Heat and Mass Transfer 2002; **45**: 2587–2595.
[7] Cabal A, Szumbarski J, Floryan JM. Numerical simulation of flows over corrugated walls. Computers and Fluids 2001; **30**: 753–776.
[8] Balaras E. Modeling complex boundaries using an external force field on fixed Cartesian grids in large-eddy simulations. Computers and Fluids 2004; **33**: 375–404.
[9] Dalal A, Das MK. Numerical study of laminar natural convection in a complicated cavity heated from top with sinusoidal temperature and cooled from other sides. Computers and Fluids 2007; **36**: 680–700.
[10] Marchioli C, Armenio V, Soldati A. Simple and accurate scheme for fluid velocity interpolation for Eulerian–Lagrangian computation of dispersed flows in 3D curvilinear grids. Computers and Fluids 2007; **36**: 1187–1198.
[11] Vasudevaiah M, Balamurugan, K. Heat transfer of rarefied gases in a corrugated micro-channel. International Journal of Thermal Sciences 2001; **40:** 454-468.
[12] Chen CK, Cho CC. Electrokinetically-driven flow mixing in micro-channels with wavy surface. Journal of Colloid and Interface Science 2007; **312**: 470-480.
[13] Castellões FV, Cotta RM. Heat transfer enhancement in smooth and corrugated microchannels. In: Proceedings of the 7th Minsk International Seminar on Heat Pipes, Heat Pumps, Refrigerators, Invited Lecture, Minsk, Belarus, (8-11 September); 2008.
[14] Wolfram S. The Mathematica book (4th edn). Cambridge: Wolfram Media; 1999.
[15] Cotta RM. Integral transforms in computational heat and fluid flow. Boca Raton: CRC Press; 1993.
[16] Cotta RM. Benchmark results in computational heat and fluid flow: – the integral transform method. International Journal of Heat and Mass Transfer (invited paper) 1994; **16**: 381–393.
[17] Cotta RM, Mikhailov MD. Heat conduction: lumped analysis, integral transforms, symbolic computation. Chichester: Wiley; 1997.
[18] Cotta RM. The Integral transform method in thermal and fluid sciences and engineering. New York: Begell House; 1998.
[19] Santos CAC, Quaresma JNN, Lima JA. Benchmark results for convective heat transfer in

ducts: – the integral transform approach. Rio de Janeiro: Editora E–Papers; 2001.
[20] Cotta RM, Santos CAC, Quaresma JNN, Pérez Guerrero JS. Hybrid integral transforms in convection–diffusion: recent applications in internal flow simulation (invited lecture). In: Proceedings of the Fourth International Conference on Computational Heat and Mass Transfer, Paris–Cachan, France, 2005.
[21] Cotta RM, Mikhailov MD. Hybrid methods and symbolic computations. In: Handbook of numerical heat transfer (2nd edn), Minkowycz WJ, Sparrow EM, Murthy JY (eds). New York: Wiley; 2006, 493–552.
[22] Pérez Guerrero JS, Cotta RM. Integral transform solution for the lid-driven cavity flow problem in streamfunction-only formulation. International Journal for Numerical Methods in Fluids 1992; **15**: 399–409.
[23] Carvalho TMB, Cotta RM, Mikhailov MD. Flow development in entrance region of ducts. Communications in Numerical Methods in Engineering 1993; **9**: 503–509.
[24] Machado HA, Cotta RM. Integral transform method for boundary layer equations in simultaneous heat and fluid flow problems. International Journal of Numerical Methods for Heat and Fluid Flow 1995; **5**: 225–237.
[25] Pérez Guerrero JS, Cotta RM. Integral transform solution of developing laminar duct flow in Navier–Stokes formulation. International Journal for Numerical Methods in Fluids 1995; **20**: 1203–1213.
[26] Figueira da Silva E, Cotta RM. Benchmark results for internal forced convection through integral transformation. International Communications in Heat and Mass Transfer 1996; **23**: 1019–1029.
[27] Pérez Guerrero JS, Cotta RM. Benchmark integral transform results for flow over a backward–facing step. Computers and Fluids 1996; **25**: 527–540.
[28] Lima JA, Pérez Guerrero JS, Cotta RM. Hybrid solution of the averaged Navier–Stokes equations for turbulent flow. Computational Mechanics 1997; 19: 297–307.
[29] Quaresma JNN, Cotta RM. Integral transform method for the Navier–Stokes equations in steady three–dimensional flow. In: Proceedings of the Tenth International Symposium on Transport Phenomena, Kyoto, Japan, (November-December); 1997.
[30] Cotta RM, Pimentel LCG. Developing turbulent duct flow: – hybrid solution via integral transforms and algebraic models. International Journal of Numerical Methods for Heat and Fluid Flow 1998; **8**: 10–26.
[31] Figueira da Silva E, Cotta RM. Mixed convection within vertical parallel–plates: – hybrid solution by integral transforms. Numerical Heat Transfer Part A – Applications 1998; **33**: 85–106.
[32] Pereira LM, Pérez Guerrero JS, Cotta RM. Integral transformation of the Navier–Stokes equations in cylindrical geometry. Computational Mechanics 1998; **21**: 60–70.
[33] Machado HA, Cotta RM. Analysis of internal convection with variable physical properties via integral transformation. Numerical Heat Transfer Part A – Applications 1999; **36**: 699–724.
[34] Pérez Guerrero JS, Quaresma JNN, Cotta RM. Simulation of laminar flow inside ducts of irregular geometry using integral transforms. Computational Mechanics 2000; **25**: 413–420.
[35] Lima GGC, Santos CAC, Haag A, Cotta RM. Integral transform solution of internal flow problems based on Navier–Stokes equations and primitive variables formulation. International Journal for Numerical Methods in Engineering 2007; **69**: 544–561.
[36] Naveira CP, Lachi M, Cotta RM, Padet J. Integral transform solution of transient forced convection in external flow. International Communications in Heat and Mass Transfer 2007; **34**: 703–712.

[37] Paz, SPA, Macêdo EN, Quaresma JNN, Cotta RM. Eigenfunction expansion solution for boundary–layer equations in cylindrical coordinates: simultaneously developing flow in circular tubes. Numerical Heat Transfer Part A – Applications 2007; **52**: 1123–1149.
[38] Silva RL, Santos CAC, Quaresma JNN, Cotta RM. Hybrid solution for developing laminar flow in wavy-wall channels via integral transforms. In: Proceedings of IMECE2007, ASME International Mechanical Engineering Congress & Exposition, Paper no. IMECE2007-42965, Seattle, USA, (November 2007), 11-15.
[39] IMSL Library. (1991). MATH/LIB. Houston, TX.

Figure Captions:

Figure 1. Definition of the general irregular geometry for the problem and coordinates system.
Figure 2. Geometric and flow characteristics of the wavy wall duct analyzed.
Figure 3. Comparison of GITT results for the product fRe for different values of the Reynolds number and dimensionless duct amplitude, against numerical results of spline alternating–direction implicit method of Wang and Chen [6]: (a) Re=100 and α=0.2; (b) Re=300 and α=0.2; (c) Re=500 and α=0.1; (d) Re=500 and α=0.2.
Figure 4. Convergence behavior of the distribution of the product fRe for Re=500 and α=0.3.
Figure 5. Profiles of the product fRe for different values of the Reynolds number and dimensionless duct amplitude: (a) Re=100; (b) Re=300; (c) Re=500.
Figure 6. Convergence behavior of the evolution of the axial component velocity at the duct centerline for Re=500 and α=0.3.
Figure 7. Evolution of the axial component velocity at the duct centerline for different values of the Reynolds number and dimensionless duct amplitude: (a) Re=100; (b) Re=300; (c) Re=500.
Figure 8. Streamline patterns along the duct length for different dimensionless duct amplitude and Re=100: (a) α=0.1; (b) α=0.2; (c) α=0.3.
Figure 9. Streamline patterns along the duct length for different dimensionless duct amplitude and Re=300: (a) α=0.1; (b) α=0.2; (c) α=0.3.
Figure 10. Streamline patterns along the duct length for different dimensionless duct amplitude and Re=500: (a) α=0.1; (b) α=0.2; (c) α=0.3.

Table 1
Convergence behavior of the streamfunction at y=0.5 for Re=100 and α=0.3

x	Infinite Duct					Truncated Duct				
	NTV					NTV				
	6	**10**	**14**	**18**	**22**	**6**	**10**	**14**	**18**	**22**
0	0.6875	0.6875	0.6875	0.6875	0.6875	0.6875	0.6875	0.6875	0.6875	0.6875
3	0.7494	0.7499	0.7499	0.7499	0.7499	0.7492	0.7498	0.7499	0.7499	0.7499
3.5	0.6655	0.6657	0.6659	0.6659	0.6659	0.6655	0.6657	0.6659	0.6659	0.6659
4	0.6922	0.6919	0.6920	0.6921	0.6921	0.6922	0.6919	0.6920	0.6920	0.6920
4.5	0.7893	0.7929	0.7943	0.7945	0.7945	0.7893	0.7929	0.7943	0.7945	0.7945
5	0.7897	0.8069	0.8095	0.8098	0.8098	0.7897	0.8069	0.8095	0.8097	0.8097
5.5	0.7747	0.7928	0.7955	0.7958	0.7958	0.7747	0.7928	0.7955	0.7958	0.7958
6	0.7759	0.7876	0.7896	0.7898	0.7898	0.7759	0.7876	0.7896	0.7898	0.7898
6.5	0.8208	0.8246	0.8261	0.8262	0.8262	0.8208	0.8246	0.8262	0.8262	0.8262
7	0.8109	0.8215	0.8232	0.8234	0.8234	0.8108	0.8215	0.8232	0.8234	0.8234
7.5	0.7944	0.8053	0.8071	0.8073	0.8073	0.7944	0.8053	0.8071	0.8073	0.8073
8	0.7924	0.7993	0.8008	0.8009	0.8009	0.7923	0.7993	0.8008	0.8009	0.8009
8.5	0.8299	0.8327	0.8340	0.8341	0.8341	0.8299	0.8327	0.8341	0.8341	0.8341
9	0.8190	0.8287	0.8302	0.8304	0.8304	0.8190	0.8287	0.8302	0.8304	0.8304
9.5	0.8287	0.8129	0.8145	0.8146	0.8146	0.8029	0.8129	0.8145	0.8146	0.8146
10	0.7998	0.8064	0.8076	0.8077	0.8077	0.7998	0.8063	0.8076	0.8077	0.8077
10.5	0.8347	0.8373	0.8385	0.8386	0.8386	0.8347	0.8373	0.8385	0.8386	0.8386
11	0.8235	0.8327	0.8341	0.8342	0.8342	0.8235	0.8327	0.8341	0.8342	0.8342
11.5	0.8076	0.8171	0.8186	0.8187	0.8187	0.8076	0.8171	0.8186	0.8187	0.8187
12	0.8041	0.8103	0.8115	0.8116	0.8116	0.8041	0.8103	0.8115	0.8116	0.8116
12.5	0.8374	0.8399	0.8411	0.8411	0.8411	0.8374	0.8399	0.8411	0.8411	0.8411
13	0.8261	0.8351	0.8364	0.8365	0.8365	0.8261	0.8351	0.8364	0.8365	0.8365
13.5	0.8103	0.8194	0.8208	0.8209	0.8209	0.8103	0.8194	0.8208	0.8209	0.8209
14	0.8057	0.8116	0.8128	0.8129	0.8129	0.8057	0.8116	0.8128	0.8128	0.8128
14.5	0.8328	0.8350	0.8362	0.8362	0.8362	0.8328	0.8349	0.8362	0.8362	0.8362
15	0.7733	0.7807	0.7819	0.7821	0.7821	0.7733	0.7807	0.7819	0.7821	0.7821
20	0.7448	0.7472	0.7476	0.7477	0.7477	0.7483	0.7508	0.7513	0.7514	0.7514

Table 2
Convergence behavior of the streamfunction at y=0.5 for Re=300 and α=0.2

x	Infinite Duct					Truncated Duct				
	NTV					NTV				
	10	**14**	**18**	**22**	**26**	**10**	**14**	**18**	**22**	**26**
0	0.6875	0.6875	0.6875	0.6875	0.6875	0.6875	0.6875	0.6875	0.6875	0.6875
3	0.7346	0.7347	0.7347	0.7347	0.7347	0.7346	0.7347	0.7347	0.7347	0.7347
3.5	0.6784	0.6785	0.6785	0.6785	0.6785	0.6784	0.6785	0.6785	0.6785	0.6785
4	0.6840	0.6839	0.6840	0.6840	0.6840	0.6839	0.6839	0.6840	0.6840	0.6840
4.5	0.7186	0.7191	0.7203	0.7207	0.7207	0.7186	0.7191	0.7203	0.7206	0.7207
5	0.7186	0.7262	0.7291	0.7299	0.7299	0.7186	0.7262	0.7291	0.7299	0.7299
5.5	0.7140	0.7228	0.7259	0.7267	0.7267	0.7140	0.7229	0.7259	0.7267	0.7268
6	0.7180	0.7242	0.7264	0.7270	0.7270	0.7180	0.7242	0.7264	0.7270	0.7270
6.5	0.7373	0.7399	0.7414	0.7419	0.7419	0.7373	0.7398	0.7414	0.7419	0.7419
7	0.7348	0.7405	0.7429	0.7434	0.7434	0.7348	0.7406	0.7423	0.7434	0.7434
7.5	0.7295	0.7358	0.7379	0.7385	0.7385	0.7295	0.7358	0.7379	0.7385	0.7385
8	0.7312	0.7358	0.7374	0.7379	0.7379	0.7312	0.7358	0.7374	0.7378	0.7378
8.5	0.7466	0.7489	0.7503	0.7507	0.7507	0.7466	0.7490	0.7503	0.7507	0.7507
9	0.7435	0.7488	0.7509	0.7514	0.7514	0.7435	0.7489	0.7509	0.7514	0.7514
9.5	0.7381	0.7439	0.7459	0.7463	0.7463	0.7381	0.7439	0.7458	0.7463	0.7463
10	0.7389	0.7432	0.7447	0.7451	0.7451	0.7389	0.7432	0.7447	0.7451	0.7451
10.5	0.7527	0.7550	0.7563	0.7567	0.7567	0.7527	0.7550	0.7563	0.7567	0.7567
11	0.7493	0.7545	0.7564	0.7568	0.7568	0.7493	0.7545	0.7564	0.7568	0.7568
11.5	0.7438	0.7494	0.7512	0.7516	0.7516	0.7439	0.7494	0.7512	0.7516	0.7516
12	0.7442	0.7484	0.7498	0.7502	0.7502	0.7442	0.7484	0.7498	0.7502	0.7502
12.5	0.7570	0.7593	0.7605	0.7609	0.7609	0.7570	0.7593	0.7605	0.7609	0.7609
13	0.7535	0.7584	0.7603	0.7607	0.7607	0.7535	0.7585	0.7601	0.7606	0.7607
13.5	0.7476	0.7529	0.7547	0.7551	0.7551	0.7476	0.7529	0.7547	0.7551	0.7551
14	0.7463	0.7505	0.7517	0.7520	0.7520	0.7463	0.7502	0.7517	0.7520	0.7520
14.5	0.7515	0.7535	0.7547	0.7551	0.7551	0.7515	0.7535	0.7547	0.7551	0.7551
15	0.7071	0.7129	0.7147	0.7150	0.7150	0.7079	0.7129	0.7147	0.7151	0.7151
20	0.7332	0.7356	0.7364	0.7366	0.7366	0.7350	0.7375	0.7383	0.7385	0.7385

Table 3
Convergence behavior of the streamfunction at y=0.5 for Re=500 and α=0.1

x	Infinite Duct					Truncated Duct				
	NTV					NTV				
	6	**10**	**14**	**18**	**22**	**6**	**10**	**14**	**18**	**22**
0	0.6875	0.6875	0.6875	0.6875	0.6875	0.6875	0.6875	0.6875	0.6875	0.6875
3	0.7128	0.7138	0.7140	0.7141	0.7141	0.7128	0.7138	0.7140	0.7141	0.7141
3.5	0.6850	0.6861	0.6862	0.6862	0.6862	0.6850	0.6861	0.6863	0.6862	0.6862
4	0.6856	0.6853	0.6851	0.6851	0.6851	0.6855	0.6852	0.6851	0.6851	0.6851
4.5	0.6928	0.6939	0.6938	0.6945	0.6945	0.6928	0.6940	0.6938	0.6945	0.6945
5	0.6883	0.6914	0.6943	0.6955	0.6958	0.6883	0.6914	0.6943	0.6955	0.6958
5.5	0.6829	0.6879	0.6913	0.6925	0.6927	0.6829	0.6880	0.6913	0.6925	0.6927
6	0.6882	0.6908	0.6929	0.6937	0.6939	0.6882	0.6908	0.6929	0.6937	0.6939
6.5	0.6959	0.6986	0.6994	0.7004	0.7005	0.6959	0.6986	0.6994	0.7004	0.7005
7	0.6918	0.6961	0.6992	0.7003	0.7006	0.6918	0.6961	0.6992	0.7003	0.7006
7.5	0.6866	0.6926	0.6959	0.6970	0.6972	0.6866	0.6926	0.6959	0.6970	0.6972
8	0.6914	0.6948	0.6970	0.6978	0.6979	0.6914	0.6948	0.6970	0.6978	0.6979
8.5	0.6985	0.7017	0.7027	0.7037	0.7038	0.6985	0.7017	0.7027	0.7037	0.7038
9	0.6944	0.6990	0.7021	0.7033	0.7036	0.6944	0.6990	0.7021	0.7033	0.7036
9.5	0.6894	0.6955	0.6988	0.7000	0.7002	0.6894	0.6955	0.6988	0.7000	0.7002
10	0.6937	0.6974	0.6997	0.7005	0.7007	0.6937	0.6974	0.6997	0.7005	0.7007
10.5	0.7005	0.7039	0.7050	0.7060	0.7062	0.7005	0.7039	0.7050	0.7060	0.7062
11	0.6964	0.7012	0.7044	0.7055	0.7058	0.6964	0.7012	0.7044	0.7055	0.7058
11.5	0.6914	0.6977	0.7010	0.7022	0.7024	0.6914	0.6977	0.7010	0.7022	0.7024
12	0.6955	0.6994	0.7017	0.7026	0.7028	0.6955	0.6994	0.7017	0.7026	0.7028
12.5	0.7019	0.7056	0.7068	0.7079	0.7080	0.7019	0.7056	0.7068	0.7079	0.7080
13	0.6979	0.7027	0.7060	0.7072	0.7075	0.6979	0.7027	0.7060	0.7072	0.7075
13.5	0.6927	0.6990	0.7024	0.7037	0.7038	0.6927	0.6990	0.7024	0.7037	0.7038
14	0.6958	0.6996	0.7019	0.7029	0.7029	0.6958	0.6996	0.7019	0.7029	0.7029
14.5	0.6978	0.7009	0.7019	0.7030	0.7031	0.6978	0.7009	0.7019	0.7030	0.7031
15	0.6736	0.6768	0.6795	0.6805	0.6808	0.6736	0.6768	0.6795	0.6805	0.6808
20	0.6977	0.6990	0.6999	0.7004	0.7004	0.6981	0.6994	0.7003	0.7008	0.7009

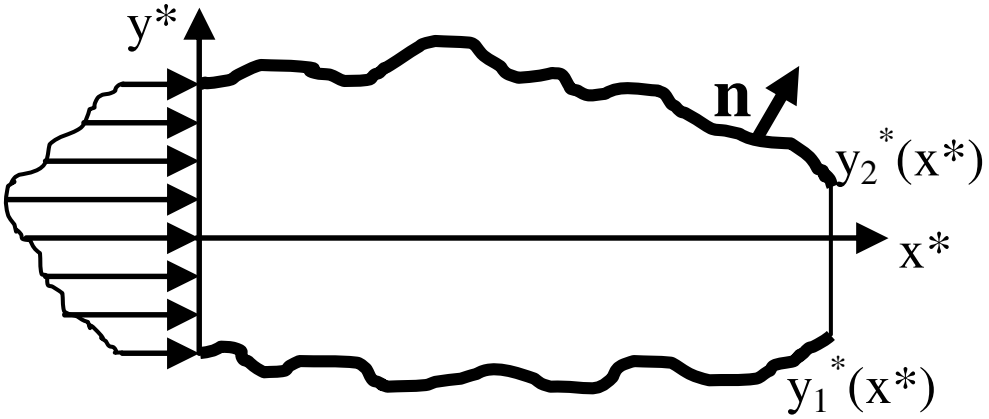

Figure 1

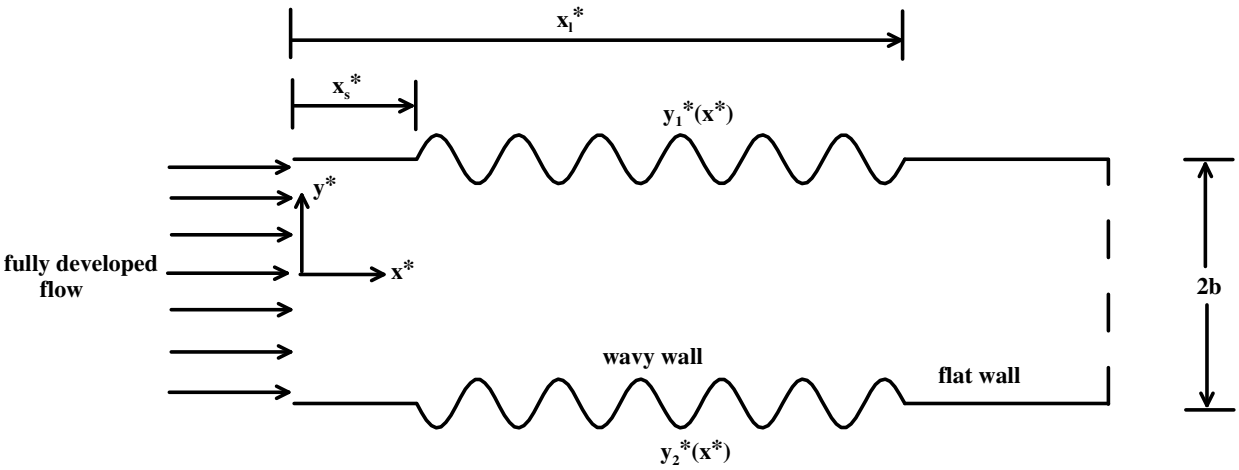

Figure 2

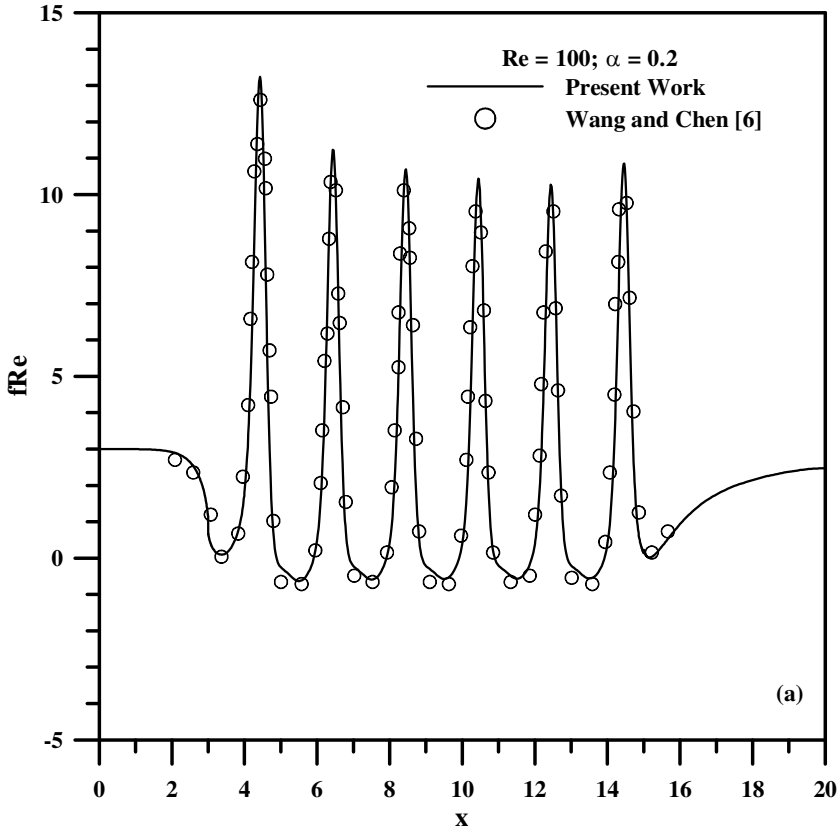

Figure 3(a)

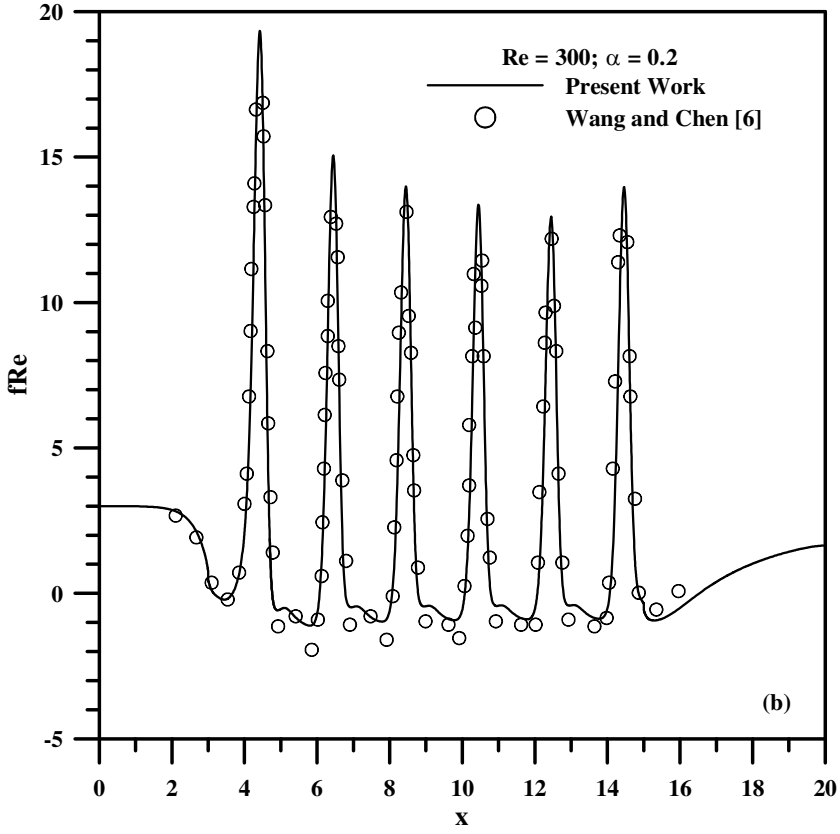

Figure 3(b)

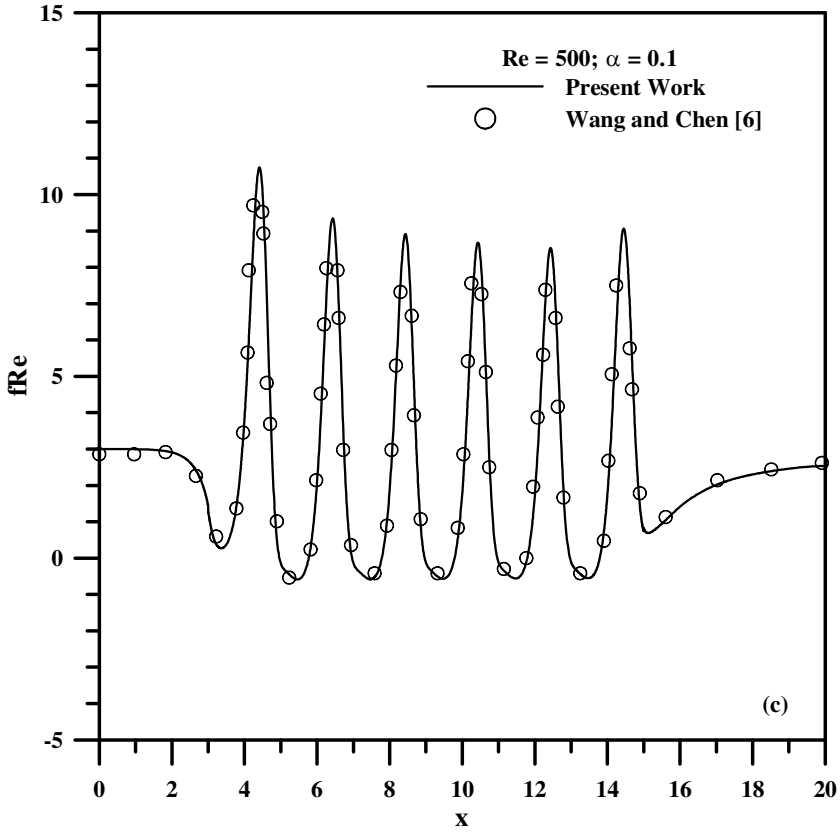

Figure 3(c)

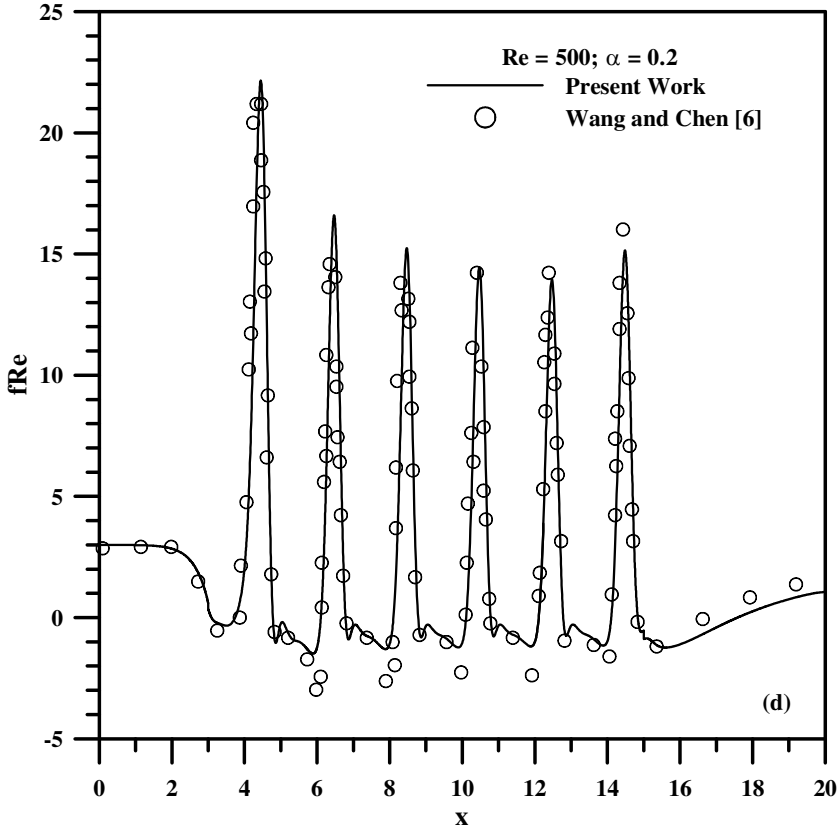

Figure 3(d)

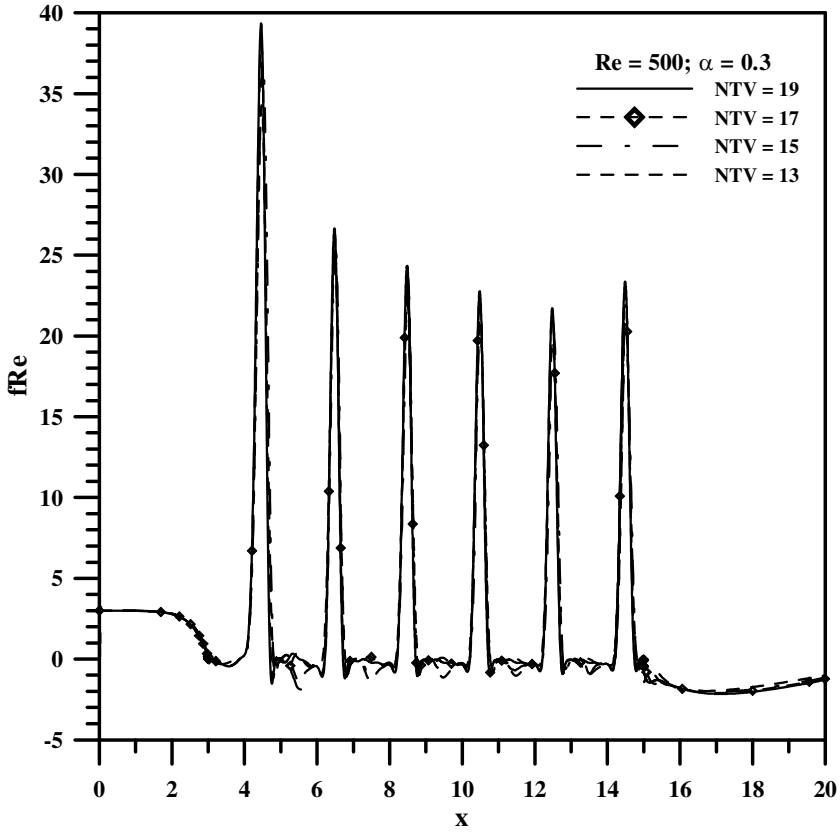

Figure 4

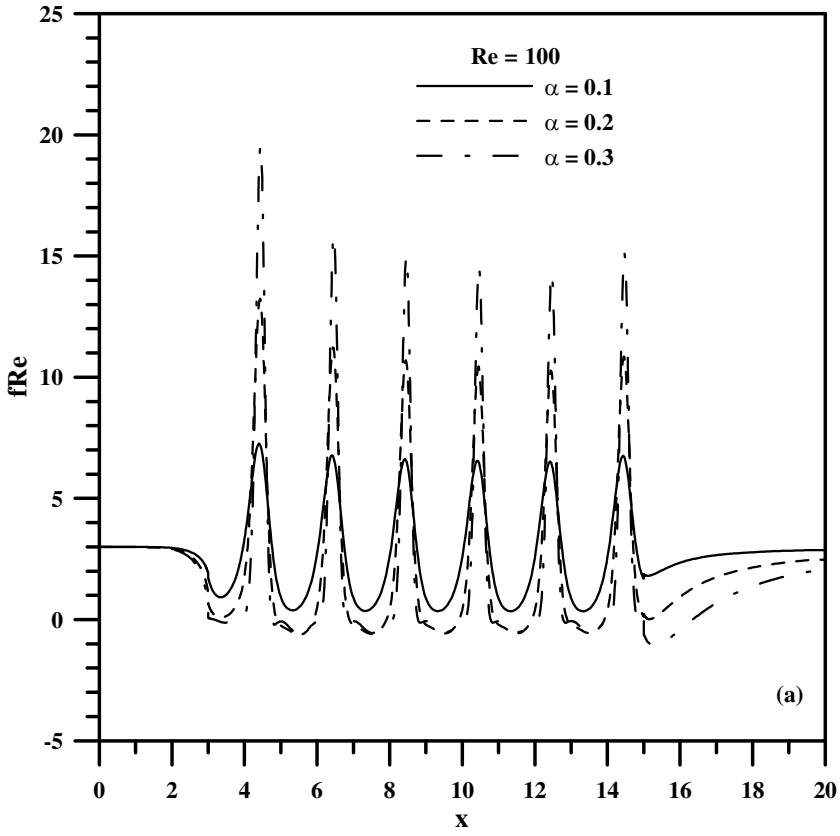

Figure 5(a)

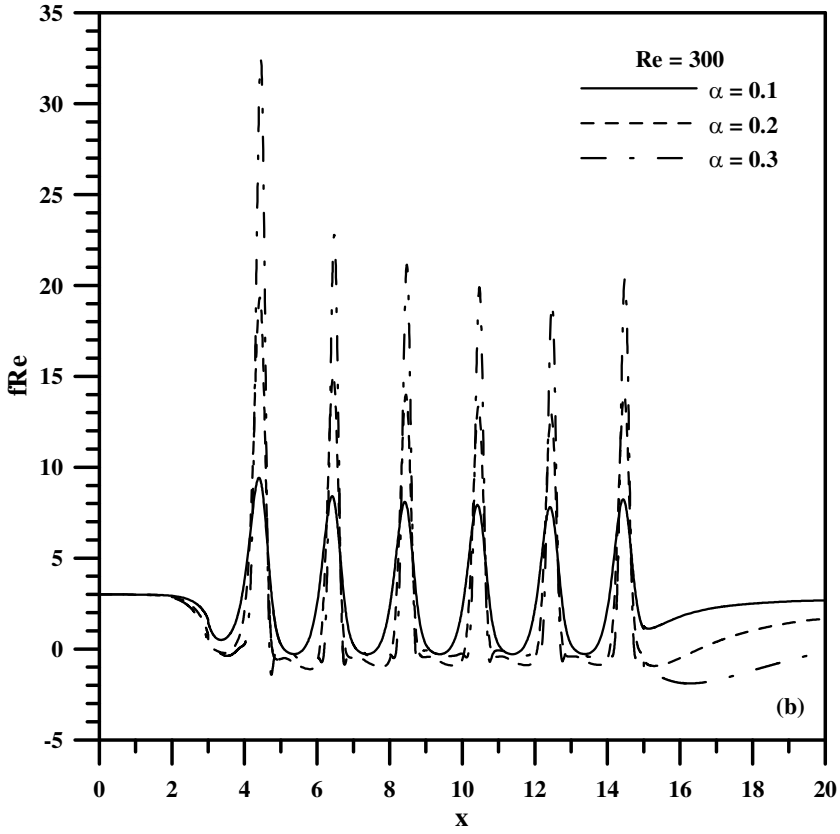

Figure 5(b)

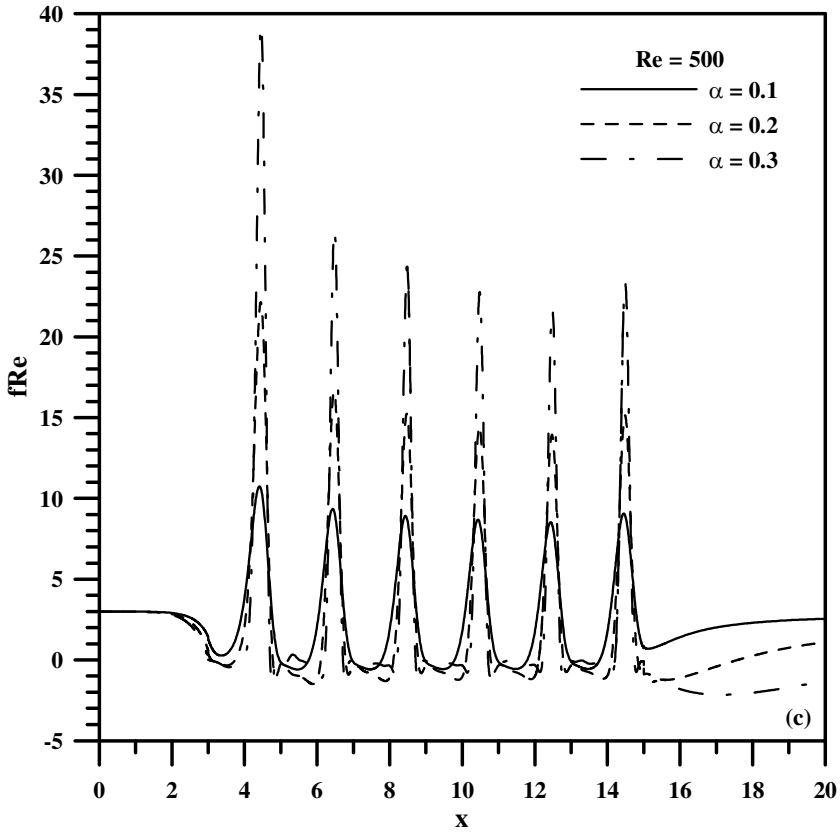

Figure 5(c)

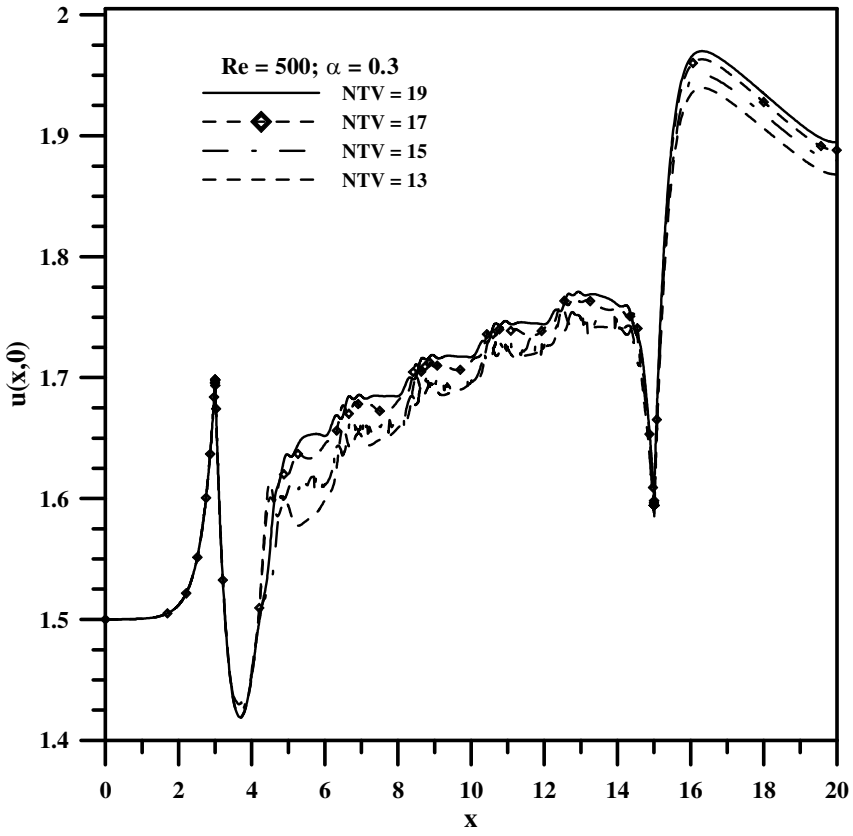

Figure 6

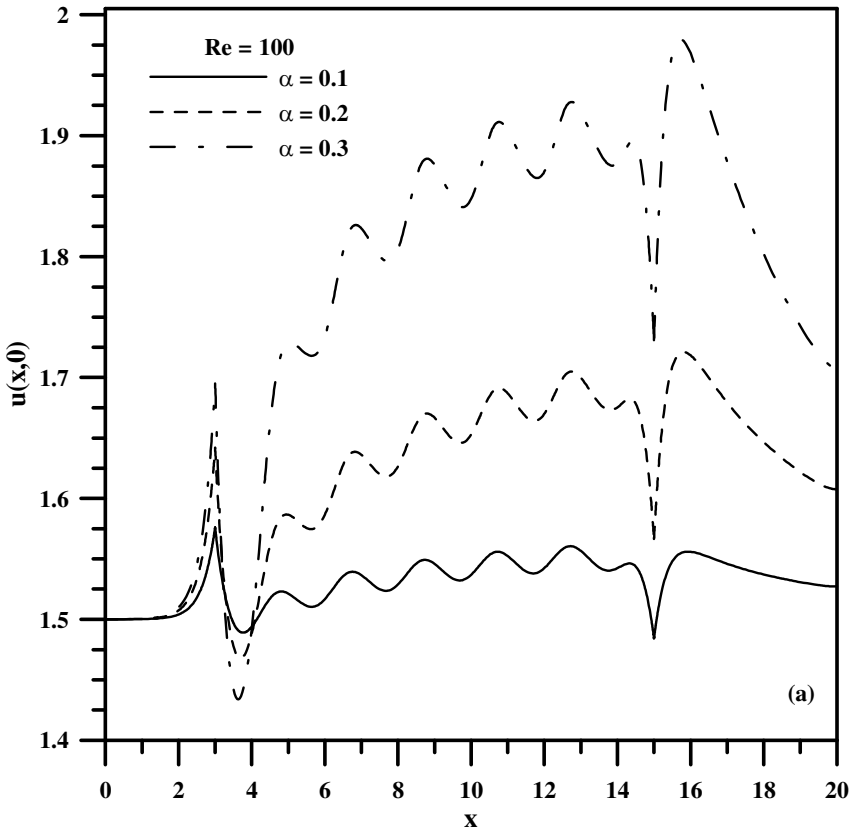

Figure 7(a)

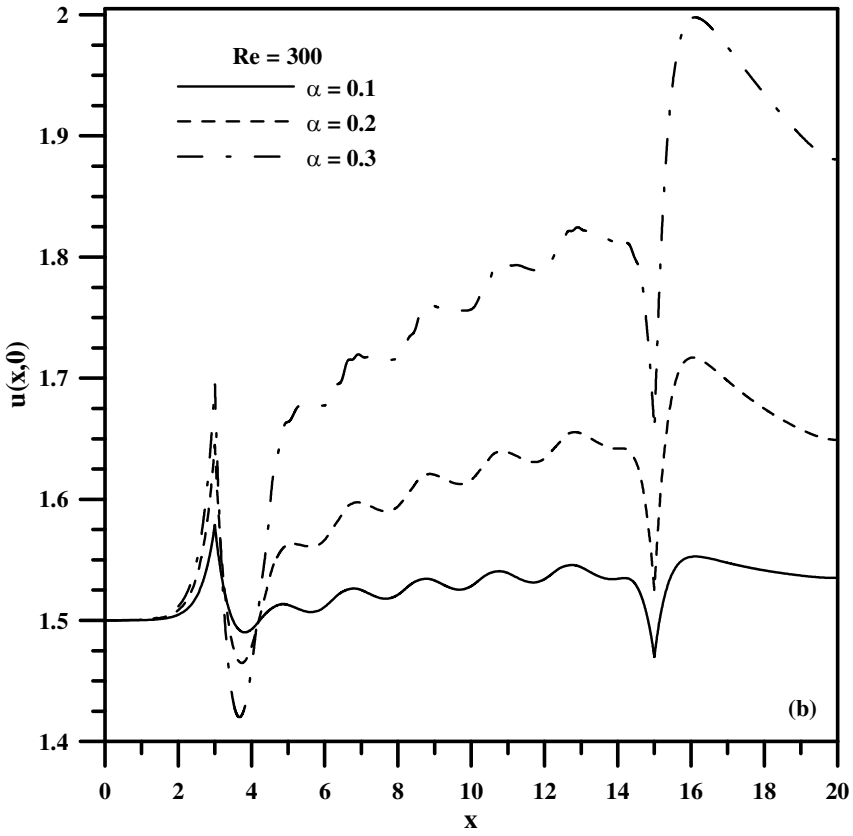

Figure 7(b)

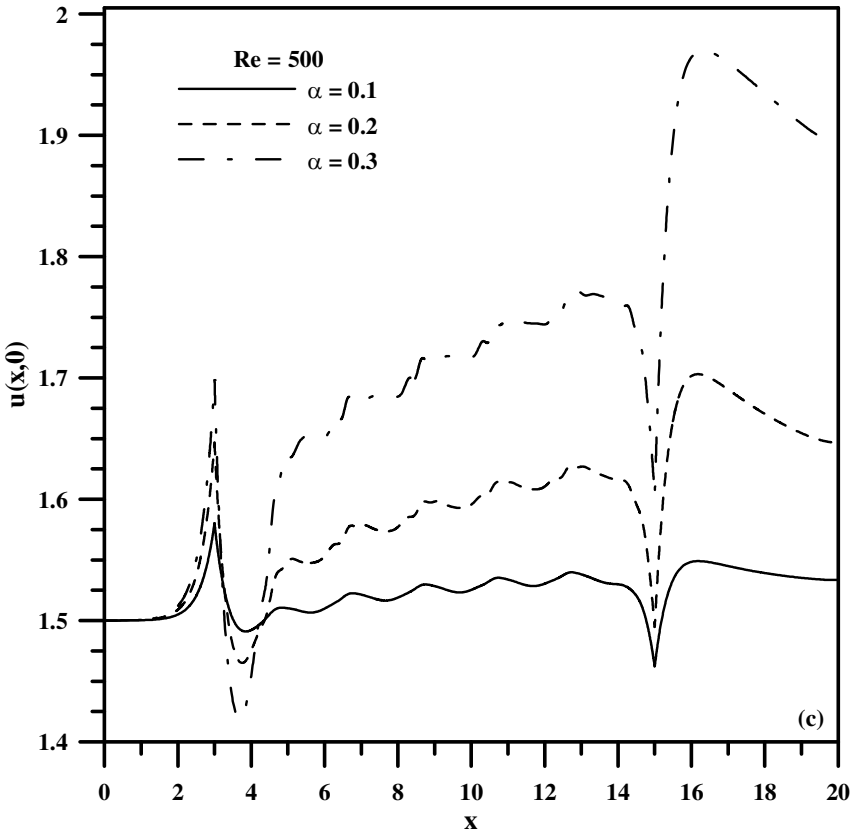

Figure 7(c)

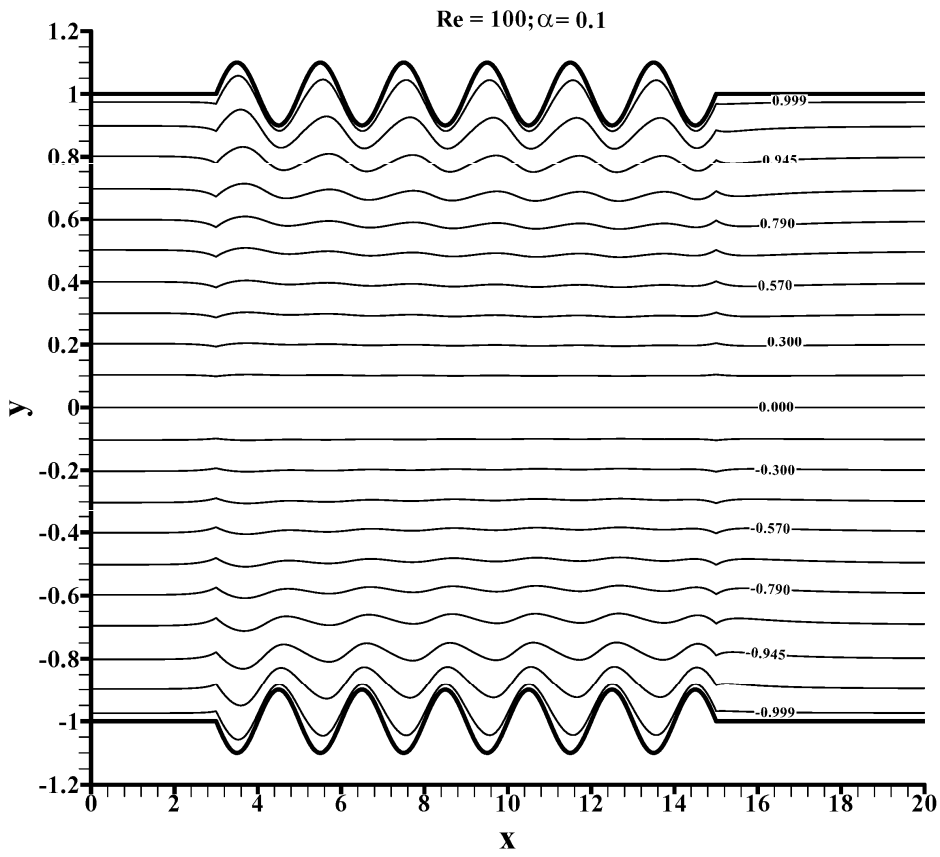

Figure 8(a)

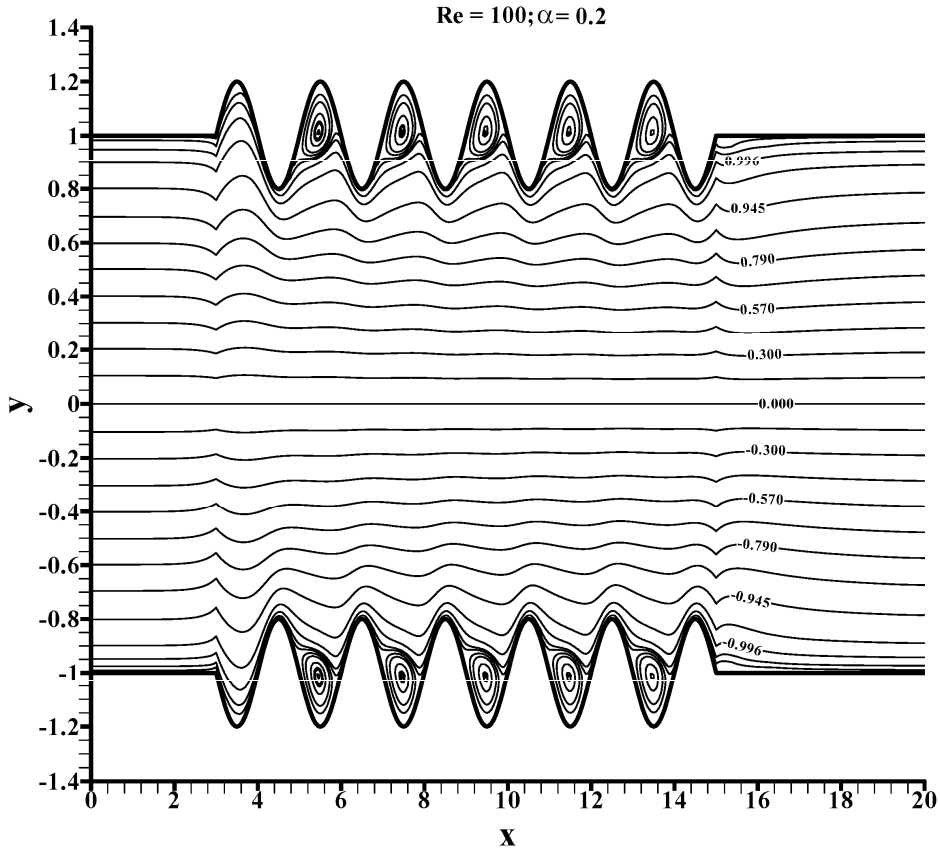

Figure 8(b)

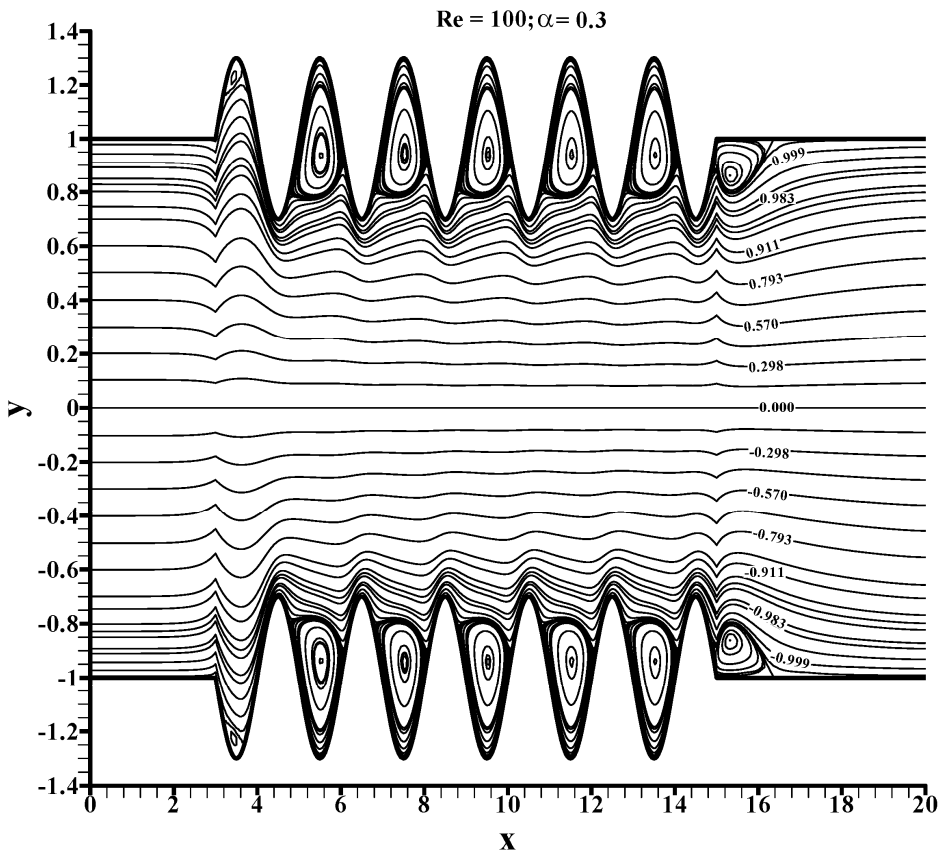

Figure 8(c)

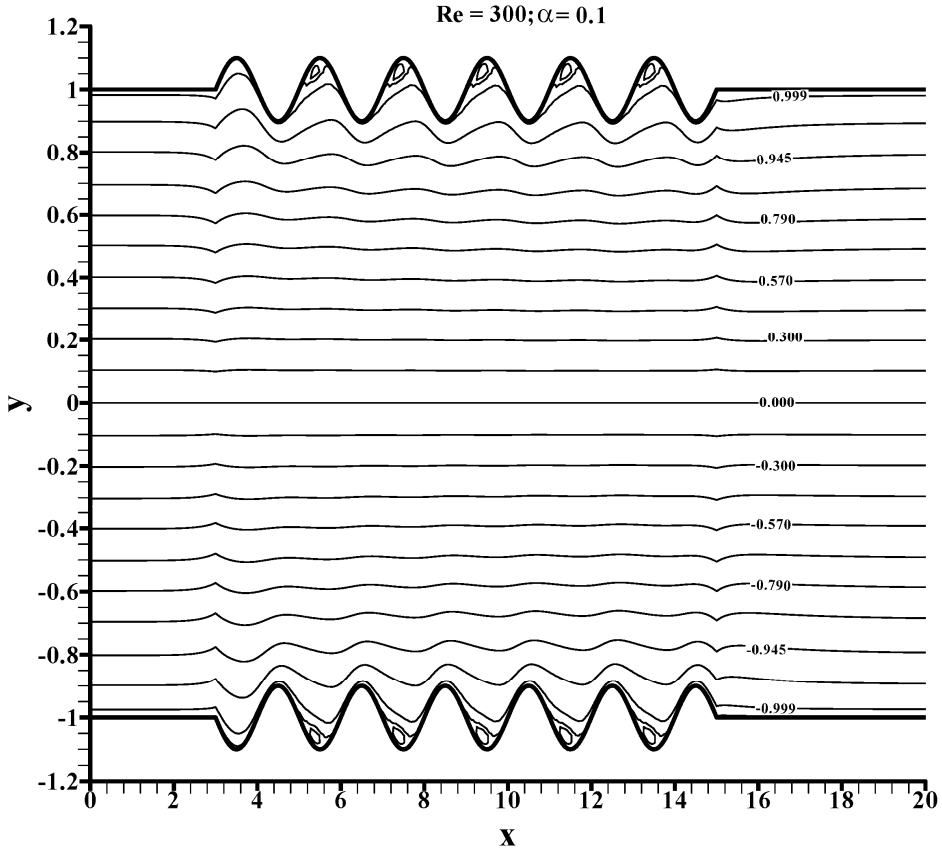

Figure 9(a)

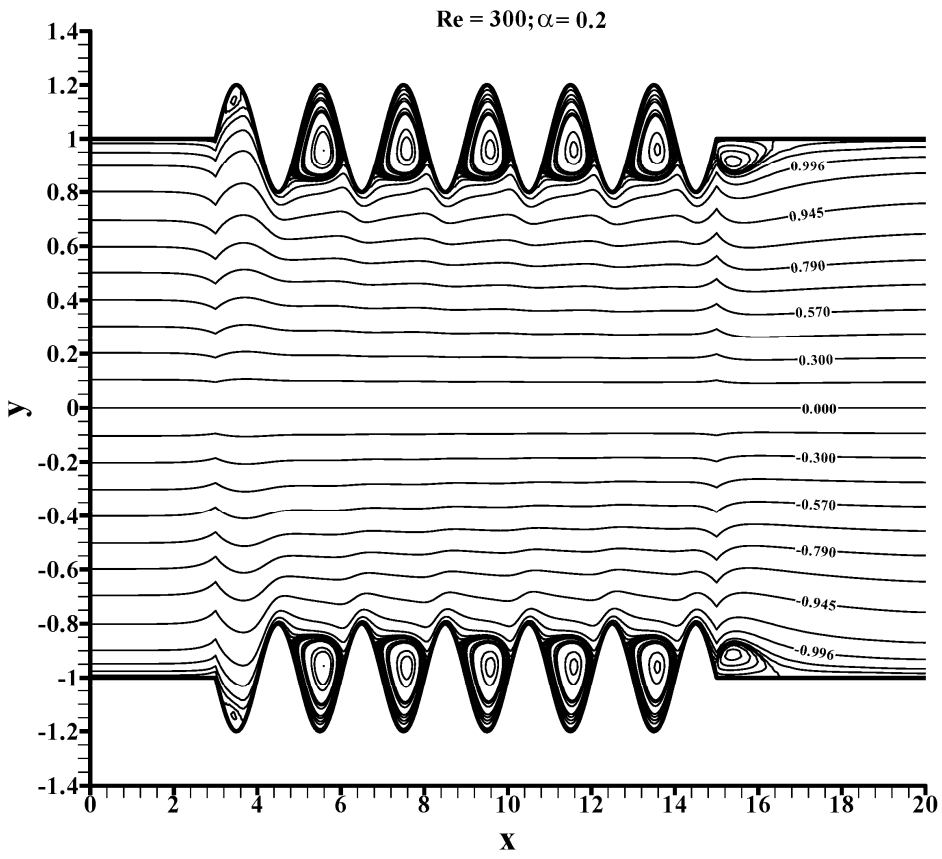

Figure 9(b)

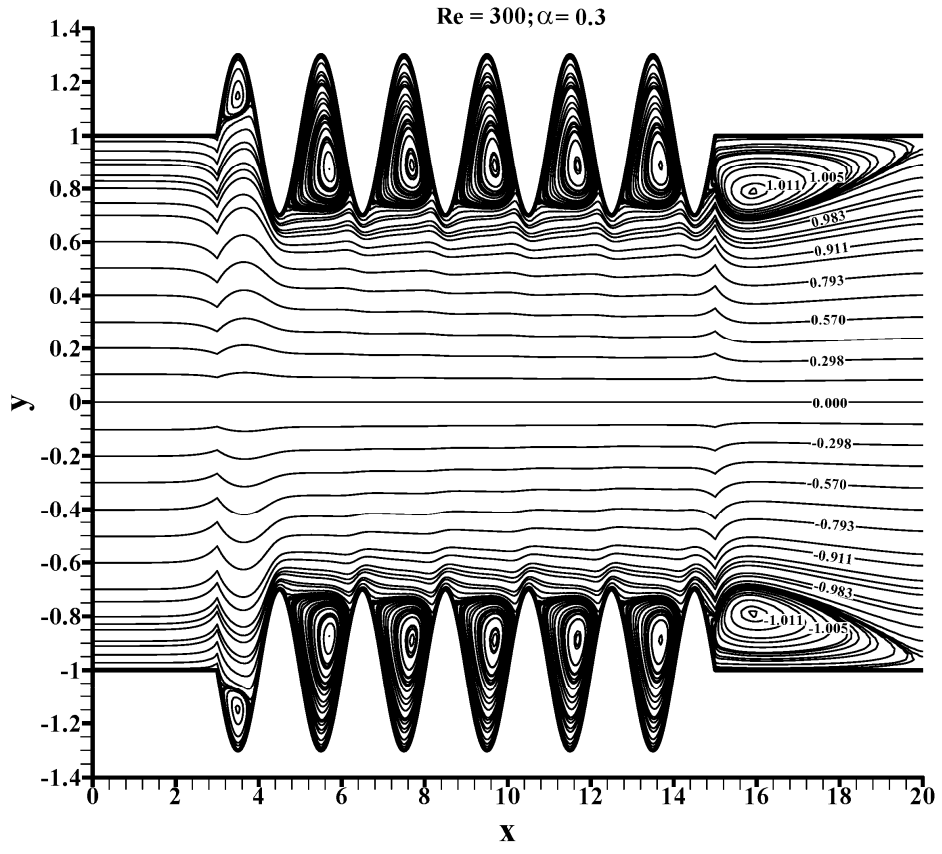

Figure 9(c)

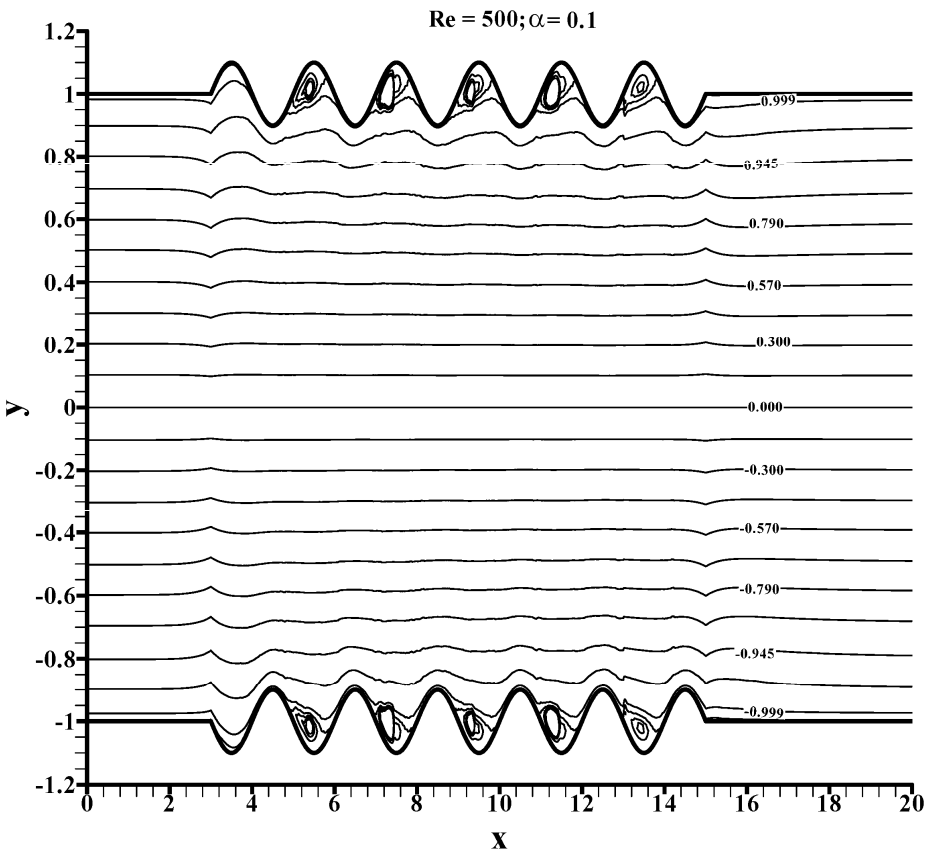

Figure 10(a)

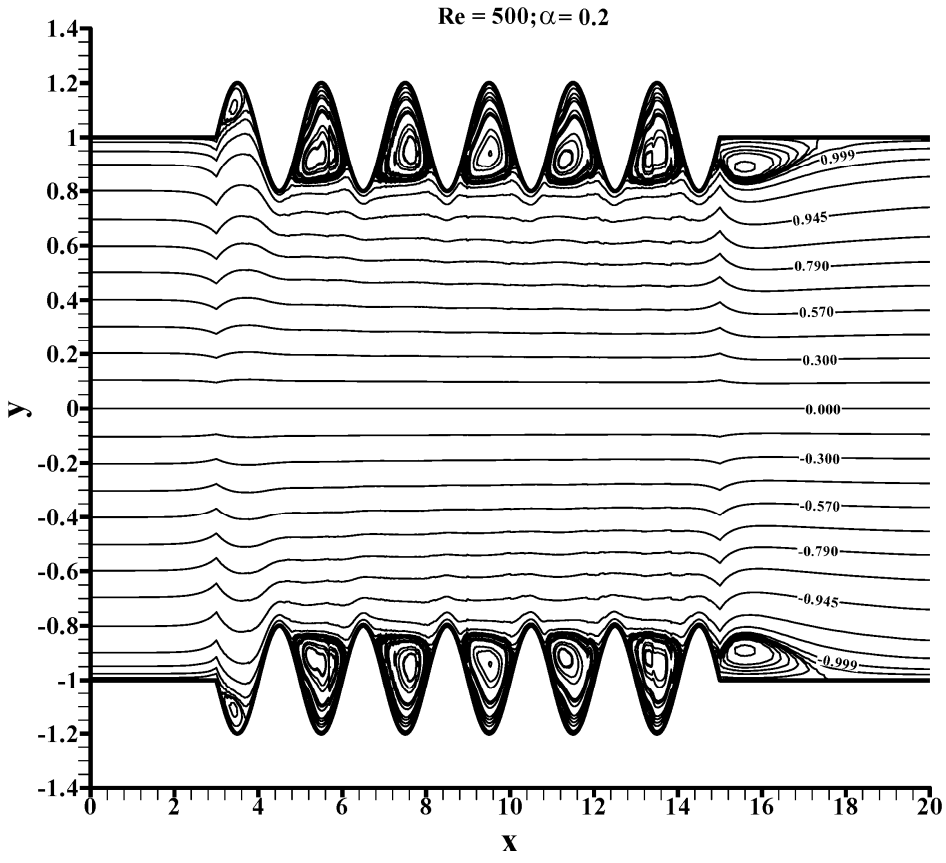

Figure 10(b)

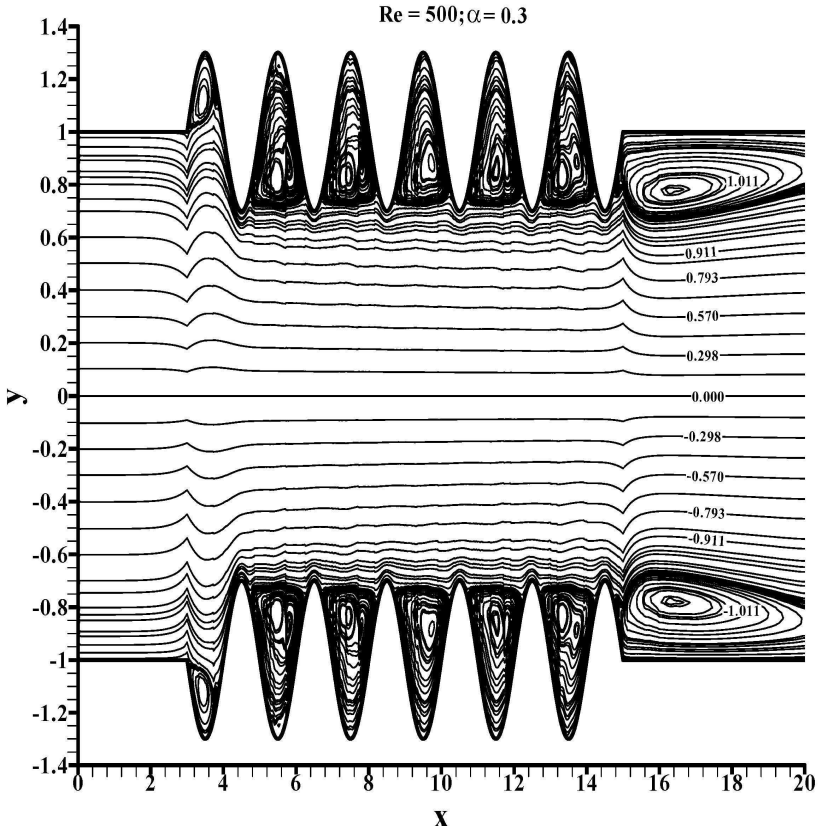

Figure 10(c)